5-10-2019

Printable Thin-Film Sol-Gel Lead Zirconate Titanate (PZT) Deposition Using NanoJet and Inkjet Printing Methods

Amanda R. Marotta
arm7402@rit.edu

RIT

Printable Thin-Film Sol-Gel Lead Zirconate Titanate (PZT) Deposition Using NanoJet and Inkjet Printing Methods

By

Amanda R. Marotta

A Thesis Submitted in Partial Fulfillment of the Requirements for the Degree of

Master of Science

In

Chemistry

School of Chemistry and Materials Science

College of Science

Rochester Institute of Technology

Rochester, NY

May 10, 2019

School of Chemistry and Materials Science

Rochester Institute of Technology

Rochester, New York

This is to certify that the Master's Thesis of

Amanda R. Marotta

has been approved by the Thesis Committee as satisfactory for the thesis requirement for the Master of Science degree at the convocation of

May 2019

Thesis Committee:

_____

Dr. Scott Williams, Primary Thesis Advisor

_____

Dr. Michael Coleman, Graduate Program Coordinator

_____

Dr. Denis Cormier Committee Member, Kate Gleason College of Engineering

_____

Dr. KSV Santhanam, Committee Member, SCMS

_____

Dr. John-David Rocha Committee Member, SCMS

_____

Dr. Gerald Takacs Committee Member, SCMS

ABSTRACT

Lead zirconate titanate (PZT) sub-5µm thin-films deposited using NanoJet and inkjet printing techniques will be presented. PZT, a perovskite ferroelectric ceramic, possesses both electrical and mechanical properties making it well suited for sensor and actuator applications. Large-scale and additive manufacturing of PZT deposition is currently unobtainable. A novel PZT sol-gel, therefore, comprised of an alkoxide mixture, was adapted for printing. Polyethylene glycol (PEG, 200MW) was discovered to be a superior film forming aid to the PZT sol-gel composite. PEG was added to the PZT composite to prevent film cracking upon gelation and thermal sintering. A powder-based sample of the PZT sol-gel was characterized using Scanning Electron Microscopy-Energy Dispersive X-Ray Spectroscopy (SEM-EDS), and Raman Spectroscopy. The Raman spectra displayed wavelength peaks around $200cm^{-1}$, $400cm^{-1}$, and $800cm^{-1}$ which indicated the desired 52/48 PZT molar ratio composite. The PZT sol-gel was printed into a thin-film using NanoJet and inkjet printing onto a cleaned stainless-steel substrate. The thin-film was thermally sintered at $700^{o}C$, and quenched in liquid nitrogen, to produce a defect-free thick film. The sub-five micron thick PZT films exhibited ferroelectric properties. This work begins to show a forward pathway for the larger scale manufacturing of device applications, such as concussion sensors, pressure sensors, and aerospace products.

ACKNOWLEDGEMENTS

LIST OF ABBREVIATIONS

Acronym	Definition
PZT	*Lead Zirconate Titanate*
TGA	*Thermal Gravimetric Analysis*
PEG	*Polyethylene glycol*
NJP	*NanoJet Printing*
AJP	*AerosolJet Printing*
SEM	*Scanning Electron Microscopy*
EDS	*Energy Dispersive X-ray Spectroscopy*
XRD	*X-ray diffraction*
MPB	*Morphotropic phase boundary*
DEA	*Diethanolamine*
MW	*Molecular weight*
IDS	*Integrated Deposition Solutions*
Au	*Gold*
FCC	*Face-centered cubic*
CTE	*Coefficient of thermal expansion*
IR	*Infrared*
cPs	*Centipoise*
NIR	*Near infrared*
UV	*Ultraviolet*
sccm	*Standard cubic centimeter/minute*

LIST OF FIGURES

LIST OF TABLES

TABLE OF CONTENTS

CHAPTER ONE-INTRODUCTION

PZT, a well-known ceramic material that shows optimal piezoelectric and ferroelectric responses, was studied. The optimal responses from the material, make it favorably used for sensor and actuator applications, and is currently considered best in its class for piezoelectric applications. A distinguishable trait of PZT, when compared to various piezoelectric materials, is that at a 52/48 (Zr/Ti) molar ratio the crystal phase composition is nearly temperature independent up to the Curie Temperature.

Additive manufacturing is the focal point of this work. Additive manufacturing is a build-up technique, unlike subtractive manufacturing, and therefore producing less waste upon manufacturing. 3D and functional printing is a subset of additive manufacturing. These printing techniques enable the fabrication of 3D and 2D structures of various materials. Functional printing facilitates the printing of materials that possess functional properties. These materials are comprised of inks that consist of either dielectrics, metals and/or nanoalloys. Functional printing is leading to the advancements in additive manufacturing which may grow to $13 billion by 2023.[1]

PZT inks are commonly prepared via a powder method. The powder method is used in additive manufacturing, due to its consistency to produce crack and defect-free PZT films, upon sintering. Several steps are involved in producing a powder-based ink. Functional printing techniques, such as NanoJet and inkjet, consist of small nozzles for ink deposition. Through the powder-based method, nozzle clogging may occur, thus preventing high-throughput of PZT films. An alternative approach is the formulation a particle-free solution or sol-gel. The sol-gel route allows for the deposition of a film with uniform molecular PZT composition. A sol-gel approach provides a facile preparation route for PZT films which minimizes any hindrances with high-throughput printing. PZT fabrication using a sol-gel method is currently not widely implemented in large-scale manufacturing.

This research focused on the formulation of an optimal PZT sol-gel composite. After designing a stable PZT sol-gel, the work would incorporate printing methods to permit thin-film deposition. Nozzle clogging for the adapted printing methods was not exhibited when implementing the PZT sol-gel. Once printed, a curing process took place to drive the gelation step

of the sol-gel synthesis. A crack and defect-free thin-film was then produced after undergoing a rapid thermal sintering process.

By taking on this research, knowledge of inorganic chemistry was expanded as well as an introduction to the field of additive manufacturing. Proper execution of this project has great potential for the manufacturing sector. Applications of a novel sol-gel PZT would expand from medical devices to instrumentations used in many labs today. Chemistry and engineering problem-solving skills were the motivational forces to develop a working PZT sol-gel that is applied to additive manufacturing. This work allows for the enhancement of knowledge in the two fast growing fields, functional printing and printed electronics.

CHAPTER TWO-THEORETICAL BASIS OF RESEARCH

2.1 PEROVSKITE MATERIALS

Gustave Rose discovered the first perovskite material, calcium titanium oxide, in 1839.[2] These perovskite materials, however, were not named after Rose, but after a mineralogist, L.A. Perovski.[2] The perovskite materials show to be highly efficient in areas of superconductivity, spintronics, and catalytic properties.[2] As mentioned previously, calcium titanium oxide is a perovskite material, yet it is also a metal oxide.[2]

Metal oxides with a general stoichiometric formula of ABO_3 may form a perovskite structure[3]. In one variation, the "A" cation is a larger cation, and where "B" is a metal ion and "O" is a halogen.[2–4] According to the general ABO_3 formula, the A cation will hold a charge of +1, +2, or +3. For PZT, this would be Pb^{+2}. The B cation is the center atom of the unit cell. This cation will hold charges larger than the A cation, and up to +5. In PZT, B cation could be either Zr, or Ti. The oxygen atoms that are surrounding the cells are enlisted to balance the charges of the perovskite material, bringing the material into its natural cubic shape.[4,5,6]
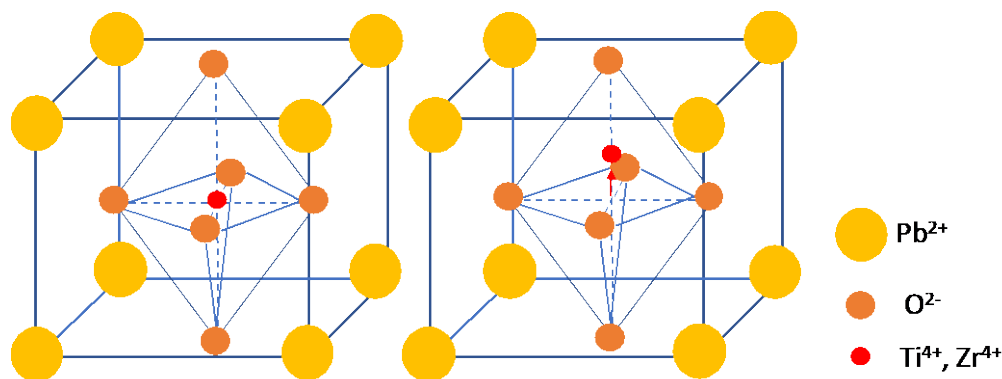
Figure 1.General schematic image of a PZT perovskite crystal in cubic form.

These perovskite materials form a crystal structure, which are atoms arranged in an ordered pattern and repeated three-dimensionally.[5] When a perovskite has a repetitive, basic, atomic group, it is referred to as a unit cell. An ideal shape of a perovskite material is considered to be a simple cubic lattice, which occurs when no external mechanical force or electrical field is applied to the crystal. If an external force or field, however, is applied to a crystal, certain lattices, such as a rhombohedral or tetragonal, are formed.[2–5]

2.2 PIEZOELECTRICITY AND FERROELECTRICITY

When a mechanical force or electric fields are applied to a perovskite material, perovskites exhibit an electrooptic, ferroelectric, and/or piezoelectric property.[13,16] Piezoelectric material properties are dependent on the direction of the lattice point location of the crystal structure. [5] From the crystal lattices, the nature of the piezoelectric material is related to the specific number of electric dipoles within the structure. Particular molecular groups with electrical properties can induce these dipoles, as well as by ions on the crystal lattice sites with asymmetric charge surroundings. Being that a dipole is understood to be a vector, the direction and magnitude of the vector relates to the electrical charges around.

The dipole moment direction can be altered when a mechanical impairment occurs.[5] This relates to the piezoelectric effect, which will be explained later, in the aspect that from this mechanical stress, the change in the polarization can change the electric dipoles. That is, the larger the mechanical variation, the larger the change in polarization, which creates a larger production of electricity.

Each crystal with a dipole moment takes on the shape of a symmetrical tetragonal or rhombohedral.[5] Perovskite ceramic crystals, when mechanically or electrically distorted, take on these shapes and the change in the dipole vector can be exhibited as a variation of surface charge density upon the face of the crystal.

French physicists Jacques and Pierre Curie first reported the piezoelectric effect in 1880.[2,5] The word piezoelectric originates from the root word piezo, in Greek, which means push. This can be related to the mechanical force or electrical field that can be applied to the crystal structure. The piezoelectric effect is the linear relationship between the stress and strain of a perovskite material. [2,5,7]

The piezoelectric effect is separated into two parts; the direct and the inverse effect.[2] The direct effect states that polarization charges are induced from the material in response to an external mechanical stress that is applied to the crystal. The inverse effect, however, states that the resulted polarization charge is in response from a separate external electric field that is applied to the material. The Curie brothers, however, did not predict this inverse effect, but rather Gabriel Lippman discovered this in 1881 via mathematical deductions from thermodynamic principles.

The direct and indirect effect are only exhibited from non-centrosymmetric materials. If the material is centrosymmetric, there is no piezoelectric response. Centrosymmetric structures possess inversion symmetry which would result in dipole moment cancelation. Balanced charges, leading to a zero free energy, is the natural state of the perovskite material (see Figure 2a).

In order to better understand the piezoelectric effect, an understanding of elasticity would be of use. A material is elastic when it conforms back to its original shape after distortion resulting from an external mechanical force.[5] When a mechanical force is applied to the perovskite material, the direct piezoelectric effect is displayed. Two known forces, tension or compression, can be involved here when applied to the material (see Figure 2b). When the material is strained, the charge of the material becomes unbalanced. Charge imbalance causes an increase in the free energy of the material. The perovskite will counteract this increase in free energy by inducing an opposite electric field through atomic displacement. This idea is also consistent for a material, which has been expanded (see Figure 2c).
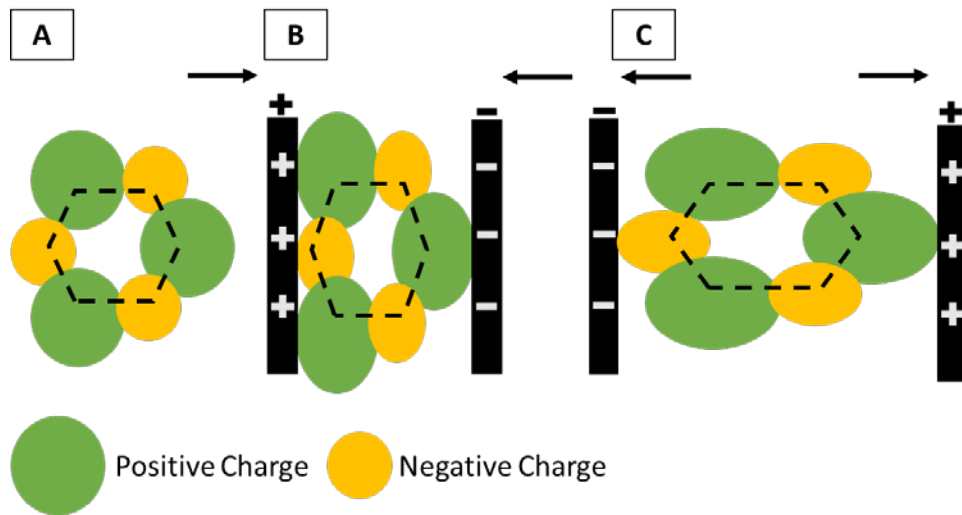
Figure 2.A perovskite material with no induced electric field (a). A perovskite material with an induced electric field (b, c).

A dielectric material is a poor electric conductor or is an electric insulating material.[9] Several piezoelectric materials are elastic, but all piezoelectric materials are dielectric. For a dielectric material, an external electric field is applied to the piezoelectric material. This causes the material to produce an unbalanced charge increasing the free energy.

To counteract this displacement, the piezoelectric material produces an opposite induced dielectric polarization (see Figure3).[5] The dielectric constant can proportionally quantify the polarization of the material
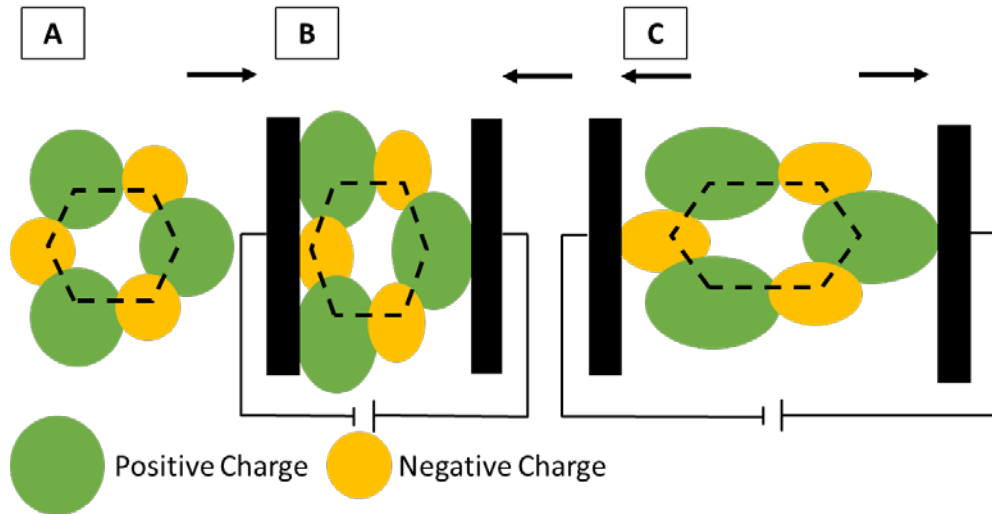
Figure 3. A perovskite material with no induced electric field (a). A perovskite material with an induced electric field via an applied external electric field (b, c)

When some materials display piezoelectric properties, they may then be categorized as a ferroelectric material. For a material to be ferroelectric, when in the absence of an electric field, the material must display a spontaneous electric polarization. When an external electric field is applied, the polarization response must be reversible.[5]

For a ferroelectric material to display its most optimal polarization response it must stay below the Curie temperature (Figure 4).
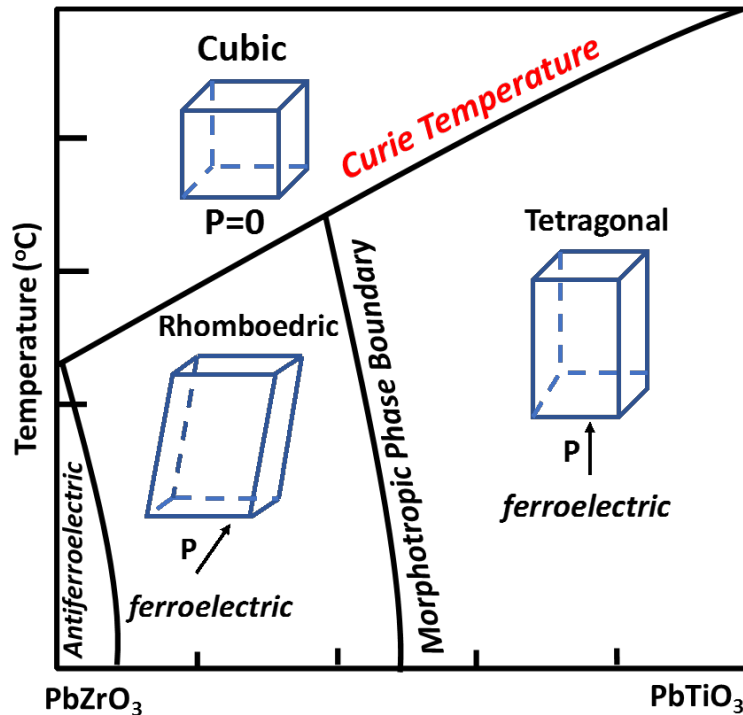
Figure 4. Displays the dependence of several phases of PZT to the Curie temperature. When the crystal lattice displays a unit cell, a cubic shaped material is formed. Above the Curie temperature the material will exhibit no ferroelectric response.

Centrosymmetric structures have inversion symmetry. Above the Curie temperature, the structure of the perovskite material is considered to be cubic and will exhibit no ferroelectric response. Below the Curie temperature, a rhombohedral or tetragonal structure forms which will exhibit a piezoelectric and ferroelectric response.[5,10] A material will display a ferroelectric response under the Curie temperature of 659 K in cases specifically for PZT.

The optimal ferroelectric or piezoelectric response falls along a morphotropic phase boundary.[5,10] Generally, this boundary line defines a separation of phases. The PZT morphotropic phase boundary (MPB) occurs when there is a ratio between the rhombohedral and tetragonal phases that will display a high ferroelectric or piezoelectric response. For PZT, specifically, a MPB is found when the Zr/Ti concentration ratio is 52/48 at room temperature.[5,10–12] A 52/48 ratio will allow PZT to be easily poled between a rhombohedral and tetragonal phase, and therefore, demonstrate a large piezoelectric response.

2.3 X-Ray Diffraction

  X-Ray Diffraction (XRD) is a characterization method used to obtain information regarding a specific crystal structure. XRD relies on the dual wave and particle nature of X-rays.[13] A monochromatic X-ray incident beam will come into contact with a sample, in this case lead zirconate titanate (PZT). The beams will scatter amongst ordered material and undergo both constructive and destructive interferences (Figure 5).
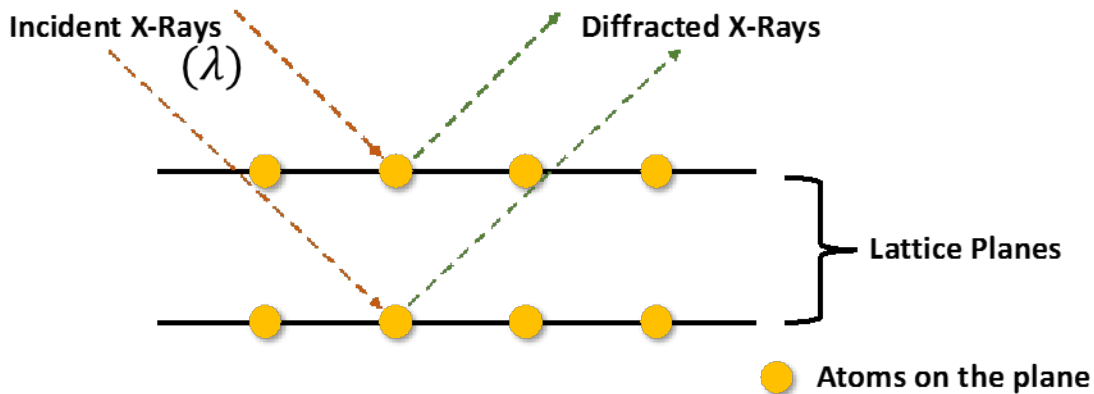
Figure 5. Schematic representation of XRD. Incident beams, λ, hit the atoms along the sample's plane and experience a destructive interference. These beams are then constructively formulated into a single peak.

  In order to have constructive interference, the extra distance that a diffracted beam will travel can be further explained through Bragg's Law, as shown below (Equation 1).

$$n(\lambda) = 2dsin(\theta) \ (Eq1)$$

Where n represents a positive integer and λ is the wavelength of the incident beams. As the incident beam hits an atom in the plane, the distance between these planes is noted as, d, and the angle at which each beam is diffracted is known as theta.

  Miller Indices are applied in XRD in order to identify directions and planes of peaks.[13] The number of indices is proportional to the dimension of the crystal lattice for the material being studied.

When studying a three-dimensional structure, a group of three numbers will indicate the orientation of the atoms along a plane in that crystal (Figure 6). These three integers are *h, k, and l*. From these integers, the families of planes can be denoted as the reciprocal lattice planes, where $\boldsymbol{G}_{(h,k,l)} = h\boldsymbol{b_1} + k\boldsymbol{b_2} + l\boldsymbol{b_3}$.
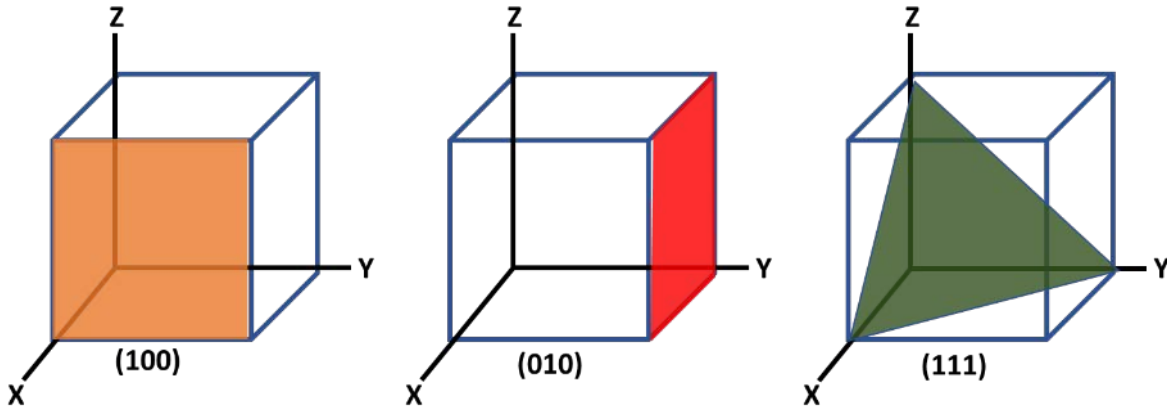
Figure 6. Coordinates of the Miller Index in a crystal unit cell.

A crystal structure has a unique XRD diffraction profile. From the XRD spectrum, the Miller indices of a material can be identified. Structural identification can be made by comparing an unknown XRD profile with published calculated data.

2.4 THERMAL ANALYSIS

Thermal gravimetric analysis (TGA) is an analytical method in which the change of sample mass is measured as a function of temperature in the gas-filled chamber.[14] TGA may provide information regarding a phase change, a temperature-dependent reaction or decomposition of a composite. The solid loading fraction of the sol-gel solutions and inks were determined using this technique.

2.5 SCANNING ELECTRON MICROSCOPY-ENERGY DISPERSIVE X-RAY SPECTROSCOPY

Scanning electron microscopy (SEM) is a technique used to image a sample displayed via a focused electron beam. The scanning electron microscope (SEM) produces visual images of samples.[15,16] SEM generates a beam of incident electrons. This electron beam is focused onto a sample, where electrons will emit from the surface and contact the electron detector to produce an image. SEM is used in conjunction with energy dispersive x-ray spectroscopy (EDS). Energy-

9

dispersive x-ray spectroscopy (EDS) provides the chemical characterization of the studied sample. This method uses the primary SEM electrons to eject an inner shell electron from the K or L shell of a surface atom. The loss of the electron from the inner shell, is filled by an electron from the outer shell. The energy (x-ray energy) difference of the shell prior to excitation and post excitation are characteristic to the atom. An x-ray detector measures the incident x-ray wavelengths. When the x-rays hit the detector, a charge pulse is formed, which is then converted to a voltage pulse. The energy is calculated from each voltage measurement. Thus, EDS can then define the elemental composition of the sample.[17]

2.6 SOL-GEL PROCESS

The ink production for this research is based on the sol-gel process. This method is used for producing solid materials from small molecules and allows for the preparation of perovskites with large surface area. For this research, an alkoxide-based sol-gel route was followed for the fabrication of metal oxides. The general sol-gel method can be seen in Figure 7.
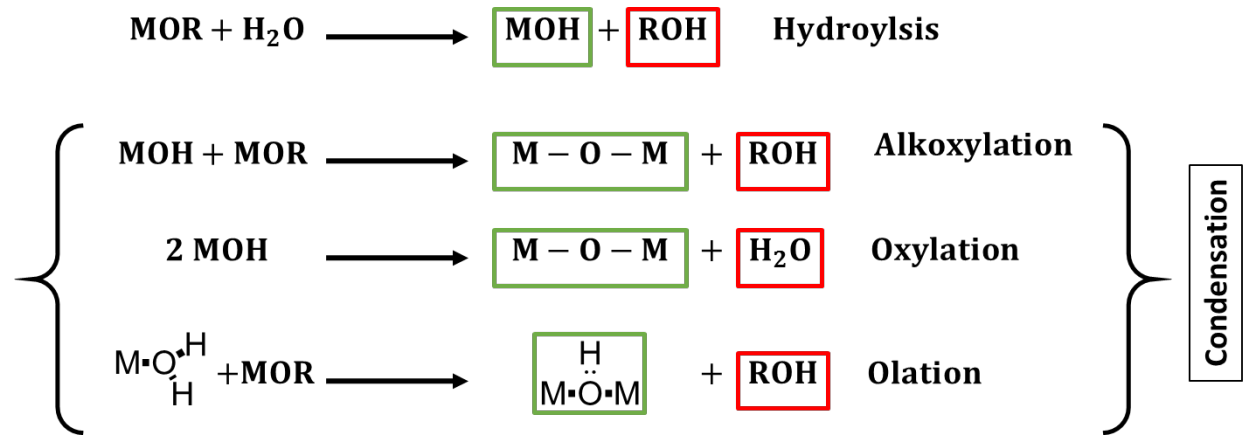
Figure 7. Chemical reaction schematic related to sol-gel process. Desired products are highlighted in green. Undesired products are highlighted in red.

During the hydrolysis reaction, a metal alkoxide ligand is hydrolyzed to form a hydroxide. In addition to the hydrolysis reaction, several condensation reactions simultaneously occur. PZT sol-gel reactions are considered to be more complex, due to the multiple metal atoms present in the molecule. Overall, the polymeric products will become insoluble via cross-linking, which in turn causes rapid gelation. Brinker and Scherer found that when the hydrolysis step is carried out with the addition of an acidic or basic catalyst, an increase in the rate of gelation occurs.[18] This

causes the polymeric products to form while simultaneously increasing the viscosity, to ultimately cause gelation.

2.7 PRINTING METHODS

2.7.1 NANOJET PRINTING

NanoJet printing (NJP) is a non-contact aerosol deposition printing technique using a low viscosity ink. The NJP method demonstrates efficiency for additive manufacturing since it can print both solid films and circuit traces smaller than 20 μm in width. NJP uses two forms of inert gas, noted as aerosol and sheath gas. The schematic printing process of NanoJet printing is shown in Figure 8.
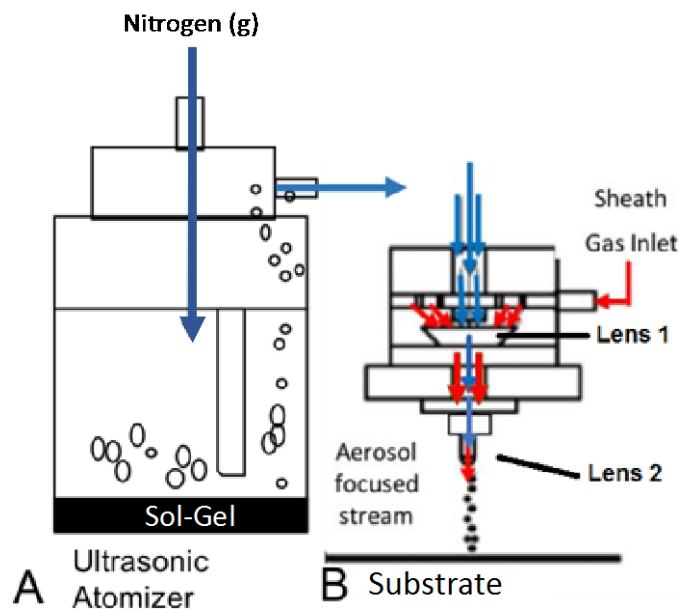
Figure 8. Schematic of the deposition head of NanoJet printer. Blue arrows represent aerosol gas, and red arrows represent sheath gas.

Similar to the commonly known Aerosol Jet printing (AJP) method, the ink that sits in the ink reservoir is atomized into aerosol droplets.[19] AJP forms aerosol droplets via either a pneumatic unit or ultrasonic unit, whereas NJP utilizes only an ultrasonic atomizer to transmit ultrasonic waves to the ink, to create the aerosol droplets (Figure 8A). These droplets are carried from the reservoir, and to the deposition head, via the pressure from the aerosol gas. Once at the deposition

head, the sheath gas is introduced to the system (Figure 8B). The sheath gas will surround both the aerosol droplets and aerosol gas, leading to a focused aerosol stream upon deposition.

2.7.2 INKJET PRINTING

Inkjet printing is considered a drop on demand digital deposition technique (Figure 9).[20] There are two major forms of inkjet print heads using either a thermal and piezo process. Thermal inkjet cartridges have a 10-20 μm square resistive heater. This causes a vapor bubble to form that is adjacent to the resistive heater. From the expansion of the bubble, a droplet of ink is forced out from the orifice. Unlike thermal inkjet, piezoelectric inkjet causes droplets via piezoelectric transducers. A voltage is applied to the transducer, which in turn bends the diaphragm. The ink sits along the diaphragm, so the action of the bend forces the ink to eject from the orifice. Droplet formation and deposition of the ink will be dependent on the surface tension of the ink. Ink viscosity is similar to NanoJet printing, in that the viscosities should be fairly low (under 10 centipoise (cPs)).
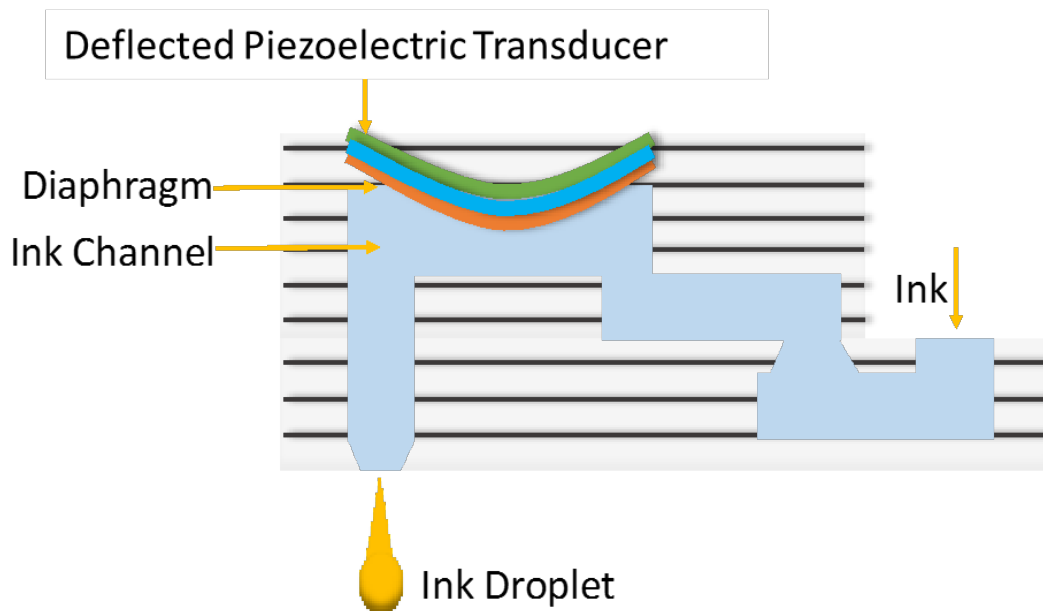
Figure 9. Schematic of the deposition head of piezoelectric inkjet printing technique.

2.8 SURFACE TENSION AND CONTACT ANGLE

When printing an ink, it is often desired to have good adhesion between the ink and the substrate. This relates to the wettability of the ink when deposited on to the desired substrate. Surface tension is the cohesive force acting along the surface of the liquid. Surface tension is usually measured along with contact angle. The contact angle can vary depending on the surface tension of the ink and the surface energy of the substrate. If a high contact angle is measured, then it is suggested that ink and substrate lack compatibility.

Inkjet and Nanojet techniques require a surface tension of approximately 20-30 dynes/cm. Surface tension is defined as the intermolecular forces that occur on the surface of a liquid.[21] The molecules within the bulk liquid are uniformly attracted to one another, resulting in a low energy state. The surface molecules, however, experience unbalanced attractive intermolecular forces, resulting in a higher energy state than the molecules in the bulk. To maintain a relatively low energy state, the surface molecules conserve a minimum surface area.

A liquid is held together through cohesive forces thereby maintaining a minimum surface area. Cohesion allows for the droplet to maintain its shape. Adhesive forces between a liquid and a surface will permit a droplet to spread, losing its shape. If the cohesive forces are greater than the adhesive forces, then the droplet will exhibit a high contact angle. For proper wetting of a liquid on a substrate, the adhesive forces must be greater than the cohesive forces.

2.9 PHOTONIC SINTERING

Photonic sintering is a short pulse sintering technique. The process implements a xenon gas-filled flash lamp that generates light between the UV to IR range. This sintering method employs high energy flash pulses to sinter the PZT film. PZT has a higher heat capacity than a metallic substrate or coated surface. The PZT will then absorb a larger proportion of the pulse energy to drive sintering processes.

Since more energy is absorbed by the PZT film, photonic sintering can help eliminate variation of coefficient of thermal expansion (CTE) values between the thin film and the substrate, which in turn may minimizes film cracking (Figure 10).[22]
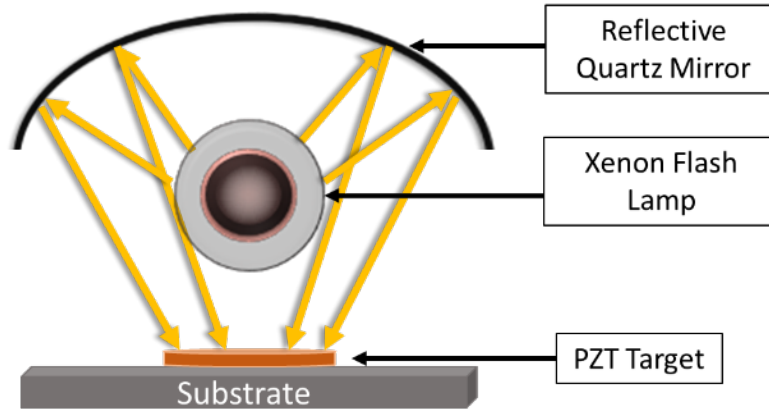
Figure 10. Schematic of photonic sinter technique.

2.10 SAWYER-TOWER CIRCUIT

A Sawyer-Tower circuit consists of two capacitors in series with each other (Figure 11).
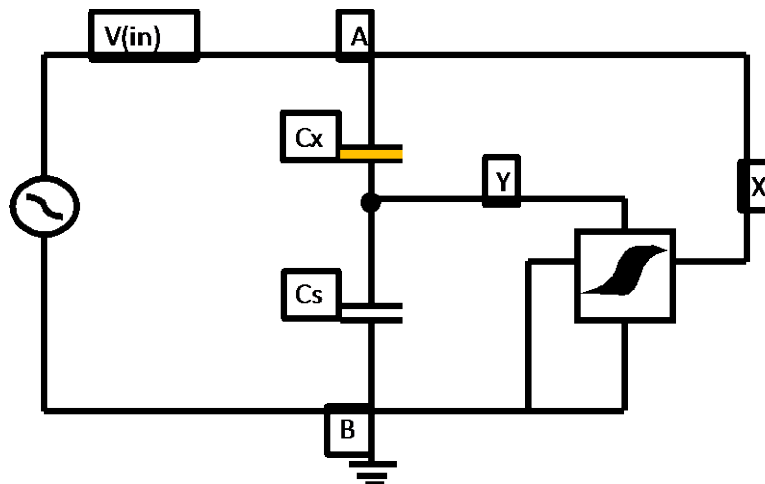
Figure 11. Sawyer-Tower circuit of two capacitors in series with each other between the stimulus signal and ground state.

Since PZT is a dielectric material, a capacitor is created and is represented by C_x. A reference or sense capacitor is noted by C_s. When the capacitance of Cs is larger than Cx, the charge remains largely localized on Cx. The charge on PZT can then be measured.[23] The Sawyer-Tower circuit is

used to measure the polarization hysteresis of many piezoelectric materials. The hysteresis generated from the circuit can correlate to the ferroelectric response of the film (see Figure 12).
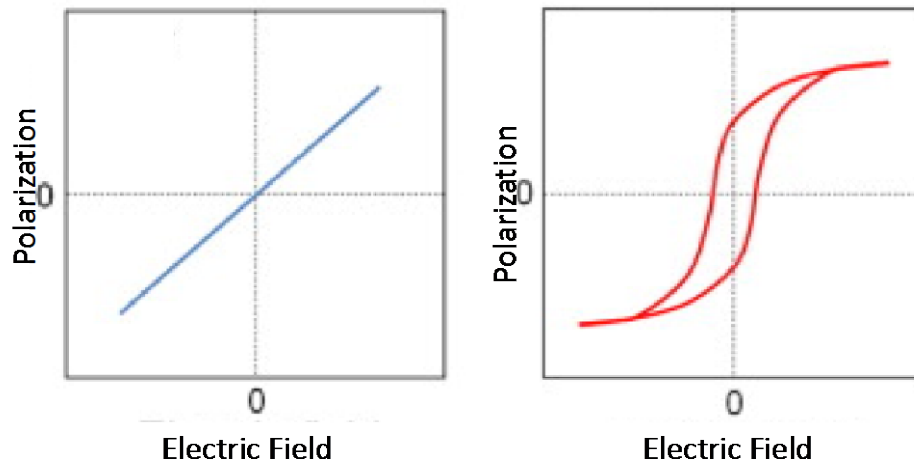
Figure 12. Hysteresis curves of ferroelectric and non-ferroelectric materials.

Based on the hysteresis effect, when in the absence of a positive or negative electric field, the material will still exhibit a remnant polarization response.
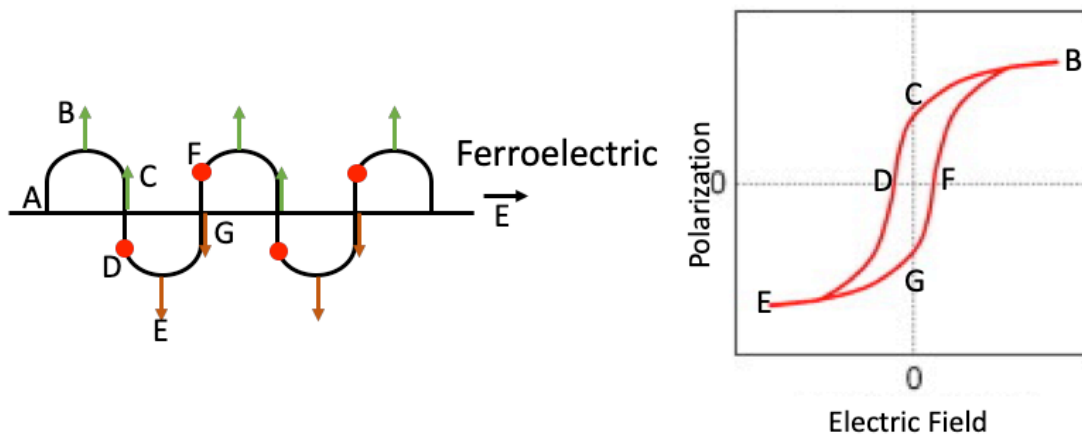
Figure 13. Depiction of a hysteresis curve produced from presence and absence of an electric field.

Figure 13 depicts a stepwise schematic of the hysteresis effect. Points B and E occur when either a positive or negative electric field has been applied to the material. Points C & G represent the measured charge stored in the material. The ability for a material to hold charge causes for a lag in measured polarization when the applied positive and negative electric field has been removed. The lag in polarization (points C and G) is known as the remnant polarization.

CHAPTER THREE- REVIEW OF THE LITERATURE

3.1 PIEZOELECTRIC MATERIALS

Piezoelectric devices have the capability to convert mechanical energy to electrical energy. Piezoelectric materials are well-suited for sensor and actuator device applications. Piezoelectric materials are a promising movement in sustainable energy due to them being highly efficient flexible and light-weight energy harvesters.[11,24] PZT is found to be the most widely used piezoelectric ceramic. PZT possesses the cubic crystal lattice of an ABO_3 metal oxide (Figure 14).
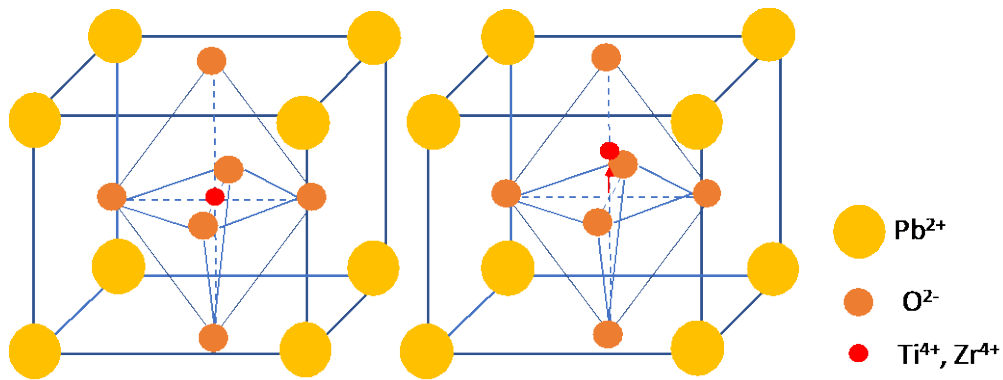
Figure 14. Crystal structure of PZT.

The general formula of PZT is Pb (Zr_xTi_{1-x}) O_3. The ferroelectric response of PZT is highly dependent on the *x* value.[25]

The optimal ratio between Zr/Ti can be found at the morphotropic phase boundary (MPB). At the MPB, both the rhombohedral and tetragonal crystal phases of PZT are present (Figure 15).
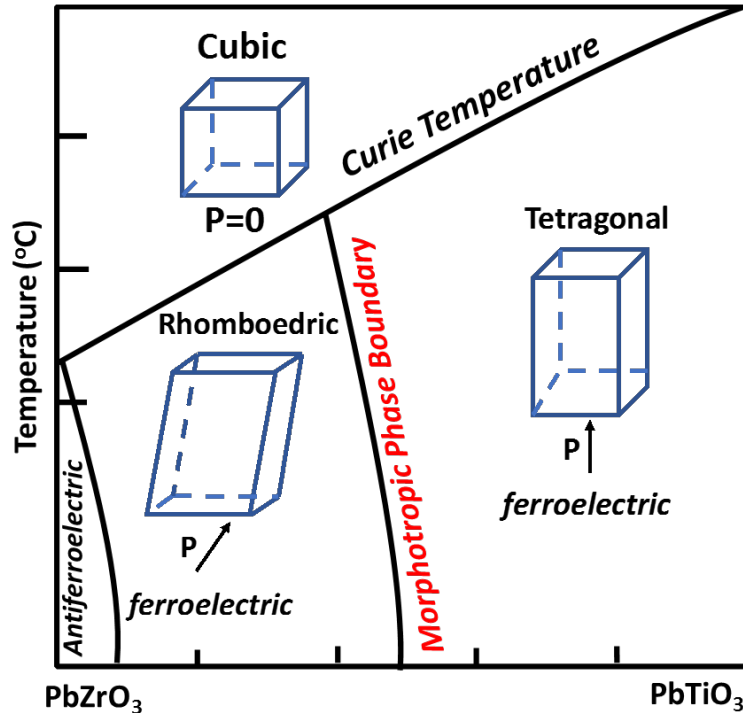
Figure 15. Phase diagram of PZT. MPB line highlighted in red.

The optimal Zr/Ti mole ratio for ferroelectric response is found to be 52/48. At this boundary, both non-centrosymmetric lattices are present (Figure 15). In contrast to other piezoelectric materials, the PZT MPB exhibits little temperature dependence. Meaning that as the temperature of the system increases, the crystalline phase composition remains relatively constant.

3.2 PZT SYNTHESIS METHODS

PZT preparation is commonly prepared using a powder-based process. In the group of Maiti, et al., they studied the synthesis of PZT using an auto-combustion process. [26] Fine particle PZT powder was produced through an auto-ignitable citrate-gel method, where TiO_2 was their starting material to decrease cost in production. The method behind the auto-ignitable citrate-gel technique was unique because its purpose was to be initiated at low temperatures. The group found that at low temperatures, thermal energy is released via an anionic oxidation-reduction reaction between citrate and nitrate ions. The group concluded that this preparation method was less

explosive than other combustion reactions, and therefore had the potential to be carried out in large scale manufacturing settings.

Similar to a powder-based method, the group of Tahar, et al., used a sol-gel preparation method to form a powder PZT composite.[27] The group used both the sol-gel and powder method to prepare PZT in order to lower sintering temperatures thereby avoiding inter-diffusion between multiple thin layers of PZT. For application purposes, low sintering temperatures would help permit silicon-based technology. The chemical reaction for preparation of PZT consisted of using diethanolamine (DEA) as a polymerizing agent to control gelation formation of the complex. As the sol-gel mechanism was carried out into a powder route, during a calcination step, an increase in crystallization at a lower temperature was observed. From these results, it was thought that forming the powder from the sol-gel prevented presence of the pyrochlore phase. However, it was later discovered that the stoichiometry of PZT was off, for the group experienced a decrease in lead content during heat processing.

Shakeri et al., explained that sol-gel technique offers an advantage in accurately controlling the molecular composition of the ceramic composite.[28] Two common types of sol-gel routes are either typical or composite. The sol-gel route is route is developed when the starting precursor materials are mixed to formulate the sol-gel solution. Whereas, the composite route entails a powder form of PZT that is suspended into a sol-gel. This method is primarily used for thick films, however, produces highly porous microstructures. Porous microstructures lead to a lower dielectric constant.

The Shakeri group then explored the typical sol-gel route. By altering the sol-gel route, using an acetic acid/alcoholic-based sol-gel, a crack-free ~45μm thick film was produced.[28] Methanol and n-butanol were added to prevent cracking of film by decreasing the solvent evaporation upon deposition. A 0.5 molar ratio of DEA and water was added to the solution. Adding DEA to the sol-gel composite introduced exothermic decomposition and combustion reactions at approximately 450 °C. These processes release a large amount of thermal energy, which suppresses the formation of pryochlore phase. By using the proposed sol-gel composite, it was concluded that a crack-free thick film with a remnant polarization of $7.8\mu C/cm^2$ was measured.

3.3 PZT DEPOSITION TECHNIQUES

Tsaur et al., implemented the sol-gel synthesis for the preparation of PZT. Tsaur's sol-gel method was favored to achieve high purity and a large volume deposition potential.[29] To better enhance the deposition of the sol-gel to various substrates, the group studied laser ablation (Figure 16).
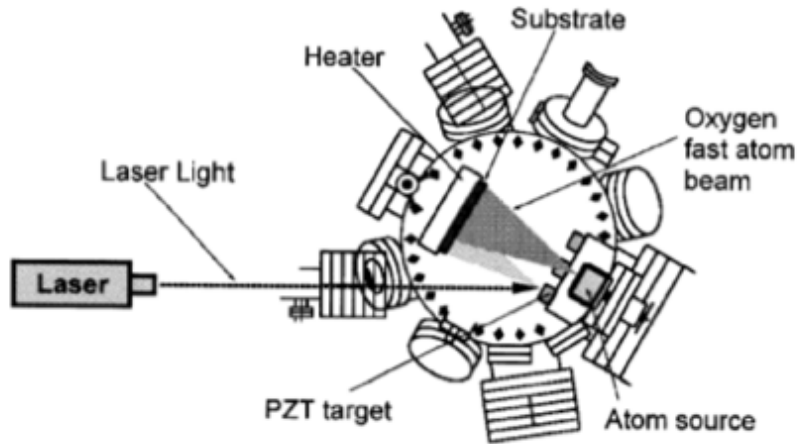
Figure 16. Laser ablation process schematic, Copyright © 2002 The Japan Society of Applied Physics.[29]

Laser ablation was intended to decrease deposition time to approximately 1-2 μm/hour. To enhance film thickness, a 3 μm film of the PZT sol-gel was spin-coated onto desired substrate and dried for a short period of time. The film was formed through a two-step sintering process. Laser ablation was then used to deposit an additional 1.65 μm of PZT. The use of laser ablation successfully increased the deposition rate of sol-gel PZT and assisted in forming a film that produced a remnant polarization of 28.6 μC/cm^2.[29]

Ouyang et al., studied the use of functional printing as the deposition technique for manufacture powder-based PZT inks. [30] Aerosol Jet printing (AJP) printing method was used. The Ouyang group was able to print PZT at speeds up to 10m/s. By repeating the printing procedure twice, PZT thick films were successfully printed at a fast rate.[30] The films were both photonically and conventionally thermally sintered.

3.4 PZT Sintering Methods

Various sintering techniques, such as laser, thermal and photonic methods, have been studied to optimize the process of PZT calcination. [27,31] Shoghi et al., uses the sol-gel preparation method from Shakeri et al., and investigates various temperatures of calcination on this sol-gel.[31] To do so, a glass-slide substrate was dip-coated in the PZT sol-gel. The sol was then dried to a gel using a hot-plate for approximately sixteen minutes. After testing temperatures from 500-650 °C, they concluded that at 600 °C, the perovskite crystallinity substantially increased, and the pyrochlore phase level was non-significant. Calcifying the film at 600 °C produced crack-free thin films.

Ouyang et al., deposited a powder-based PZT ink onto stainless steel substrates and preformed thermal and photonic sintering treatments.[30] Prior to sintering the material, the deposited films were dried in a vacuumed sealed oven for two hours at 200 °C. In a conventional furnace, argon gas flowed through the chamber to avoid oxidation. A consistent ramp up rate of 25 °C/min was carried out until the temperature reached 1000 °C. The sample incubated at this temperature for an hour, then cooled to room temperature. This method produced films with densified grains.[30] However, to decrease sintering time, photonic sintering was implemented to gather similar results.

When Ouyang et al., investigated the use of photonic sintering, the light absorbance of the PZT film was measured to be between 300-900 nm. Photonic sintering was done by exposing the sample to fifteen pulses at an applied voltage of 250 V, and pulse length of 1300 μs and frequency of 2 Hz.[30] Similar densification of grains were observed when compared to the thermally sintered material.

To compare performance of films, a Sawyer-Tower circuit was used to measure the ferroelectric hysteresis of both the thermally and photonically sintered materials (Figure 17).
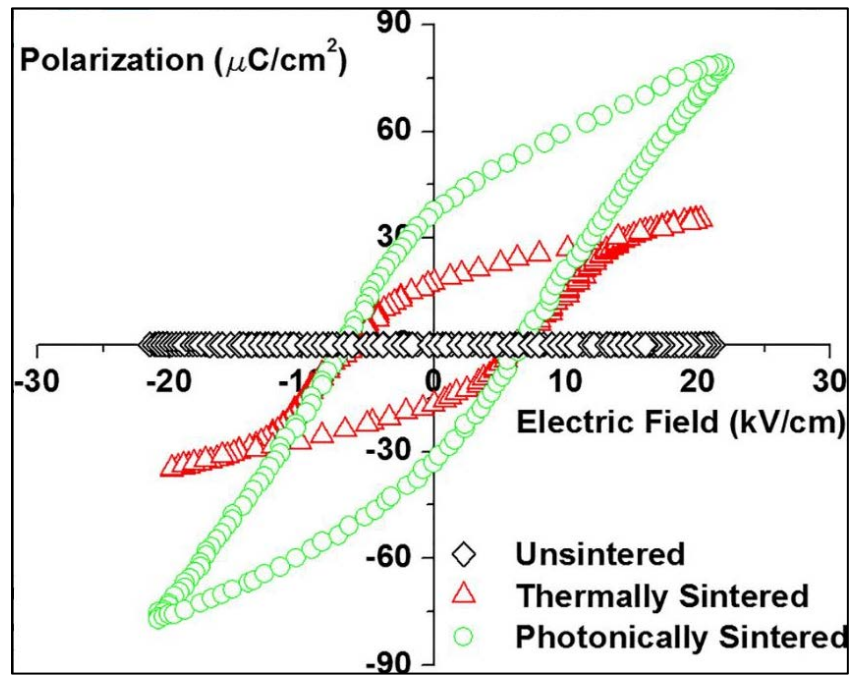
Figure 17. Hysteresis curves of thermal and photonically sintered PZT thick films, Copyright © 2016 The American Ceramic.[30]

When using photonic sintering, they concluded, that not only does it allow for the opportunity to sinter PZT in atmospheric conditions but they could also sinter PZT on low melting point substrates in short time, thus opening the door for a wider range of PZT applications.[30]

CHAPTER FOUR- PROBLEM STATEMENT

The research goal was to develop a PZT sol-gel solution for Nanojet and inkjet printing. This sol-gel was deposited onto a stainless-steel substrate as a thin-film. Nanojet and inkjet printing methods include both aerosol and digital techniques, permitting large-scale additive manufacturing. Upon deposition, the thin-film was thermally sintered into a crack-free working device. The fabricated device was studied using various analytical methods to confirm the optimal 52/48 molar ratio of Zr/Ti. This research developed a stable PZT sol-gel that was adapted to additive manufacturing.

CHAPTER FIVE- MATERIALS & METHODS

5.1 MATERIALS

All chemicals used were analytical grade. Lead (Pb) (IV) acetate trihydrate (molecular weight (MW): 379.33), Zirconium n-propoxide (molecular weight (MW): 327.57), Titanium n-propoxide trihydrate (molecular weight (MW): 284.86), polyethylene glycol (PEG) (molecular weight (MW): 200) were purchased from Sigma Aldrich, USA. These chemicals were used without further purification. Stainless-steel (SS) 430 substrates were cleaned with 1.8 M nitric acid before ink deposition.

5.2 SUBSTRATE CLEANING

1.8M nitric acid was prepared by adding 11.47 mL of nitric acid to 100 mL of distilled H_2O (dH_2O). The mixture was heated for 20 minutes at 60 ^{o}C and cooled before use. Each substrate was immersed in the final 1.8 M nitric acid wash for 20 minutes prior to printing at room temperature. Upon removal the substrates were degreased with isopropyl alcohol and dried using a lint-free wipe.

5.3 INK FORMULATION

Each ink was formulated in an argon filled glove bag and followed the same mixing process as shown in Scheme 1. All glassware was flame dried, to remove bound water, prior to being placed in an argon gas filled, glove-bag.
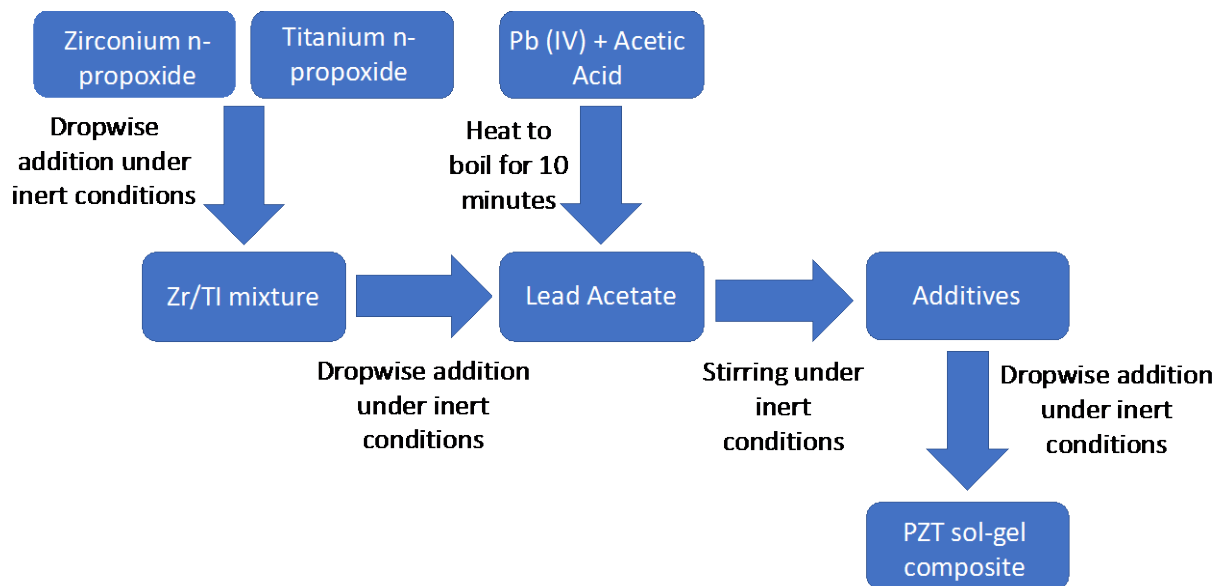
Scheme 1. Mixing process for producing sol-gel PZT.

5.3.1 STARTING PZT SOL-GEL

A Starting PZT sol-gel formulation consisted of a lead acetate solution which prepared by mixing 8.510 g of Pb (IV) acetate trihydrate and 12.64 mL of acetic acid (Table 1).

Table 1. Additive package implemented for the Starting PZT sol-gel formulation.

Additive	Mass (g)
dH_2O	0.428
Lactic Acid	0.518
Linoleic Acid	5.26
Glycerol	0.538
Ethylene Glycol	0.475

Following this, a Zr/Ti mixture under argon gas was formulated by dropwise adding 2.730 g of titanium n-propoxide to 4.960 g of zirconium n-propoxide while stirring. The sol-gel stirred for 30 minutes. While the sol-gel stirred, 0.518 g of lactic acid, 5.26 g of linoleic acid, 0.538 g of glycerol and 0.475 g of ethylene glycol were added to 0.428 g dH_2O while stirring. The prepared

additive package was slowly dropwise added into the sol-gel. The final product stirred for 60 minutes, before being removed from the glove bag. The final PZT concentration was 1.6 M.

5.3.2 MODIFIED PZT SOL-GEL

A Modified PZT sol-gel was formulated using the following process. A lead acetate solution was prepared by mixing 8.510 g of Pb (IV) acetate trihydrate and 12.64 mL of acetic acid (Table 2). A Zr/Ti mixture under argon gas was formulated by dropwise adding 2.730 g of titanium n-propoxide to 4.960 g of zirconium n-propoxide while stirring. The Zr/Ti mixture was then dropwise added into the acetate solution under inert conditions. The sol-gel stirred for 30 minutes. Then, 7.219 g of 200 MW PEG was added dropwise while stirring. After 60 minutes of stirring, the sol-gel was removed from the glove bag.

Table 2. Modified PZT sol-gel fabrication used for NanoJet printing. Final concentration of composite was 1.6M.
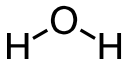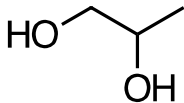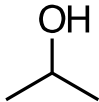
Compound	Mass (g)	Mols	Hydrolysis Steps	Mass of PEG(g)	Mols of PEG
Lead Acetate_dH$_2$O	21.78	0.2200			
Zirconium n-propoxide (Sigma Aldrich)	4.960	0.0150	Polyethylene Glycol (200MW)	7.219	0.0300
Titanium n-propoxide (Sigma Aldrich)	2.730	0.0096			

To remove hydrolysis reaction products, the PZT sol-gel was refluxed, under argon, for fifteen hours at 80 $^{\circ}$C. An acetate film formed along the wall of the glassware. Following reflux, the PZT sol-gel could be printed using the NanoJet printer or adapted for inkjet printing.

5.3.3 Optimized PZT Sol-Gel

Inkjet printing requires a specific ink surface tension; therefore, an inkjet printable ink solution was adapted to formulate the Optimized PZT sol-gel. Table 3 shows the ink vehicles used to produce the Optimized PZT sol-gel ink. Isopropyl alcohol and propylene glycol were dropwise added to 9.0 g of dH$_2$O while stirring. The solution stirred for thirty minutes before 5.0 g of the Modified PZT sol-gel was slowly dropwise added. The mixture stirred overnight.

Table 3. Optimized PZT sol-gel ink vehicles.

Material	Mass (g)
dH$_2$O	9.00
Propylene Glycol	2.51
Isopropyl Alcohol	3.50

5.3.4 Ink Rheology

Surface tension and contact angle measurements were taken of the Modified PZT sol-gel and Optimized PZT sol-gel using a Ramé Hart instrument (Model: 260-U1) with teflon tip. Viscosity measurements were based off qualitative comparison. Each sol-gel was compared visually against a sample of distilled water, which has a viscosity of 1 cPs.

5.4 Spin Coating

Preliminary results of the Starting and Modified PZT sol-gels were done using a spin casting deposition technique. A Speedline Technologies spin coater (Model: P96700) was used for this work. A dozen drops of the sol-gel was deposited onto the desired substrate. The spin casting ramp recipe consisted of three steps. For the first five seconds the spin coater was set to

1800 RPM. At ten seconds the instrument was set to 3000 RPM. After fifteen seconds the instrument decreased to 0 RPM. The recipe used permitted for a homogenous thin-film deposition of the sol-gel.

5.5 NANOJET PRINTING

The Modified PZT sol-gel was printed using an Integrated Deposition Solutions (IDS) NanoJet printer. The printer uses an ultrasonic atomizer unit with a 0.51 amp current flow. A sheath gas flow of 80 sccm and an aerosol flow of 80 sccm were chosen for film deposition. A 22-gauge nozzle was selected to deposit the ink on a stainless-steel substrate (2 mm standoff distance). The print speed was set to 2.0 mm/s. A solid square pattern (1 cm x 1 cm) was designed using AutoCad (2015) and converted into a .prg file and was used for printing.

5.6 INKJET PRINTING

The Optimized PZT sol-gel was printed using a Fuji Dimatix Inkjet printer (DMP 3000). The printer used piezoelectric, 16 nozzle ink cartridges with a 10 picolitre (pL) drop volume. The voltage applied to the piezoelectric cartridge was 24 V, while the nozzle temperatures remained at 25 $^{\circ}$C. The image printed with a file resolution set to 1270 drops/inch (dpi). A solid square film (1 cm x 1 cm) was printed on a stainless-steel substrate (1250 μm standoff distance) and sintered in a muffle furnace.

5.7 POST PROCESSING

Upon deposition of the sol-gel PZT, the thin-film was dried using a near-IR Adphos lamp at 2.0 V for approximately twenty minutes. The film was then transported to a ProMetal (Model RF-D) muffle furnace for a thermal sintering process in ambient conditions. A crack and defect-free thin-film was produced by rapidly heating up the sample at 100 $^{\circ}$C/minute to 700 $^{\circ}$C. The sample was immediately removed after one minute and quenched in liquid nitrogen.

5.8 CHARACTERIZATION

A thermal profile of the Modified PZT sol-gel was measured using TGA Q 500 (TA Instruments, USA). A ramp up rate of 10 $^{\circ}$C/minute to 800 $^{\circ}$C was set. The TGA method was done using nitrogen. The molar composition of PZT was analyzed using SEM-EDS (Jeol, JSM-IT100LA, USA) under high vacuum with an accelerating voltage of 15 kV. Raman spectroscopy

(Bruker, Senterra II, USA) was implemented for film analysis. The 532 nm laser with a power of 25 mW was selected for this study. The final, un-polled, PZT thin-film ferroelectric properties were measured using a Sawyer-Tower circuit. A voltage amplifier was used to apply a variant range of 1-6 V to the sample. The maximum voltage and frequency set, from the oscilloscope, were 5 V and 500 Hz.

CHAPTER SIX- RESULTS & DISCUSSION

When printing any ink, the process from ink to print is called the printing workflow. The printing press is blind to the ink technology. The ink technology, however, must be matched to the engineering requirements of the press. The focus of this work was to formulate a working PZT sol-gel that would possess a molar Zr/Ti ratio of approximately 52/48. To deposit the sol-gel solution using a printing method, the rheological properties required further modifications. Several sol-gel compositions were studied. A substrate was selected that would provide the most useful and stable surface to support the PZT cured film. Even when all ink and printing parameters are optimized, the PZT film must be transformed from a solution to solid state. The curing energy required must be sufficient to create a film with the paper phase, and therefore, ferroelectric properties. Chapter 6 will highlight the adjustments made to fabricate a crack and defect-free PZT working device.

6.1 INK FORMULATION

6.1.1 STARTING PZT FORMULATION

6.1.1.1 STARTING PZT FORMULATION DEPOSITED ON QUARTZ

The sol-gel solution was spin coated onto quartz substrates. Quartz is a chemically compatible material to PZT, being that they are both ceramic oxides. Quartz, also known as silicon dioxide, takes on a tetrahedral crystal structure. Quartz can exist in several polymorphic forms, one of which is face-centered cubic (fcc). PZT, at room temperature, has a simple cubic structure, however, at elevated temperatures the fcc structure is formed. Due to the crystalline phase compatibility of the quartz and PZT, both ceramics are expected to possess many common mechanical properties, such as, the degree and rate of thermal expansion.

PZT was then spin-coated onto quartz substrates, however, film cracking was still exhibited. (Figure 18).
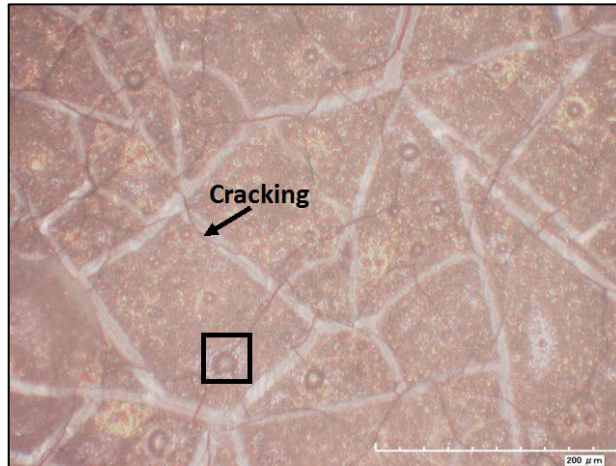
Figure 18. PZT sol-gel thermally sintered on quartz substrate (200 µm scale).

Gold (Au) shares the same fcc unit cell as PZT. Since the atoms of Au and PZT are similarly packed, the crystal growth upon thermal heating are likely comparable. Sputter coating both metals onto the quartz substrate, therefore, was done to enhance film quality (Figure 19).
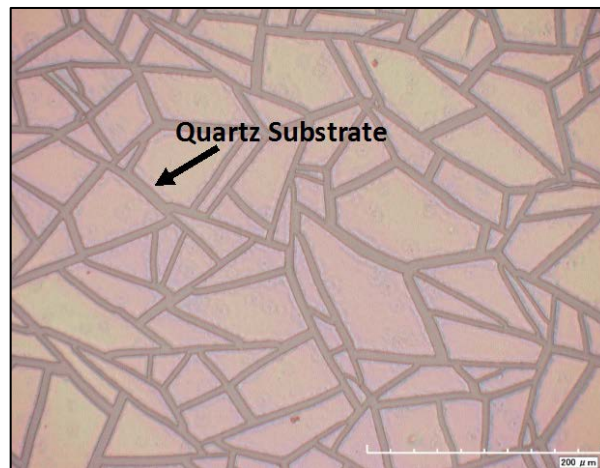
Figure 19. PZT sol-gel thermally sintered on Au sputter coated quartz substrate (200 µm scale).

Noteworthy was the absence of film cracking within the PZT film (Figure 19).

6.1.1.2 STARTING PZT FORMULATION DEPOSITED ON STAINLESS-STEEL

PZT deposited on stainless steel would permit for the low cost production of a working device. The conductivity of stainless-steel forms the basis of a working device reducing the need

for an expensive bottom electrode such as evaporated gold. The PZT sol-gel, therefore, was spin-coated onto a polished stainless-steel disk. Quartz and stainless-steel metal have significantly different thermal properties. For instance, the thermal rate of expansion of stainless-steel is 1.8×10^{-6}/ ^{o}C, whereas a typical ceramic has a rate of expansion of 10.5×10^{-6}/ ^{o}C. The PZT film may experience thermal stresses that create defects upon thermal sintering given the large CTE differences between both materials. (Scheme 2).
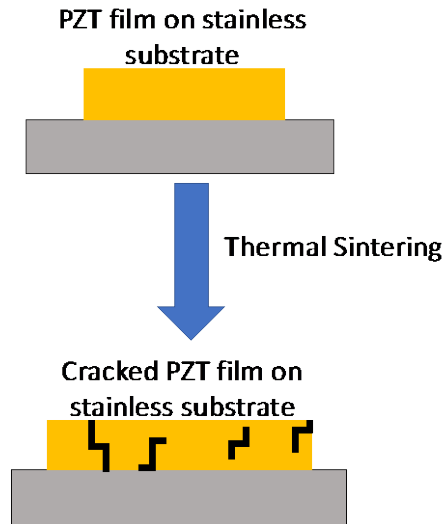
Scheme 2. Schematic of coefficient of thermal expansion (CTE) effects on PZT sol-gel deposited on stainless-steel substrate.

A PZT sol-gel spin-coated onto a stainless-steel substrate and thermally sintered at 800 ºC is shown in Figure 20.
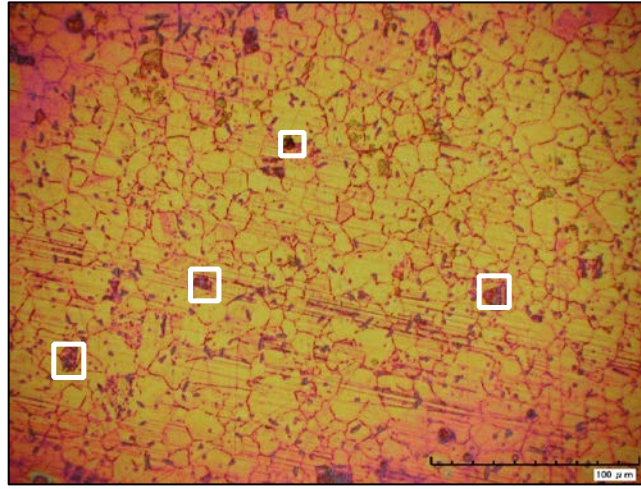
Figure 20. PZT sol-gel thermally sintered onto stainless-steel substrate. Film defects are highlighted within white squares. (100 µm scale).

As expected, based on difference in CTE values, the film contained multiple cracks and defects. Examples of some cracks and defects are highlighted in Figure 20.

In attempts to overcome the difference of CTE values of PZT and stainless, as well as, the difference in crystal structure, gold (Au) was sputtered coated onto a stainless substrate prior to PZT deposition (Figure 21).
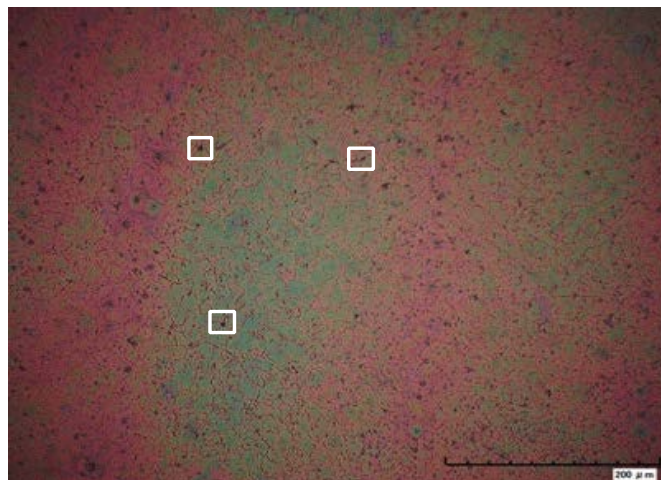
Figure 21. PZT sol-gel thermally sintered on Au sputter coated stainless-steel substrate (200 µm scale).

Examples of defects have been highlighted using white squares in Figure 21 Rather than multiple cracks among the grains, pinhole defects occurred upon thermal sintering. These results suggested that Au sputtering reduced some defects in the film.

6.1.1.3 INCOMPLETE HYDROLYSIS REACTION

Multiple failed attempts of sintering crack and defect-free PZT films were produced until the sol-gel synthesis was revisited. The reaction products in the sol-gel synthesis contained the same functional groups of those used in the additive package (Equations 2, 3)

$$MOR + H_2O \rightarrow MOH + ROH \ (Hydrolysis) \quad (Eq2)$$

$$Condensation \begin{cases} MOR + H_2O \rightarrow MOM + ROH \ (Alkoxylation) \\ 2MOH \rightarrow MOM + H_2O \ (Oxylation) \\ M - H_2O + MOR \rightarrow M_2OH + ROH \ (Olation) \end{cases} \quad (Eq3)$$
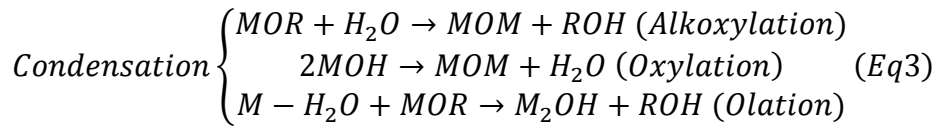
According to Le Chatlier's Principle, when adding an excess amount of product to a reaction, the reaction will be driven back towards the reactants. This effect prevents the completion of the hydrolysis reaction for the sol-gel synthesis (Eq 4).

$$MOR + H_2O \Longleftrightarrow MOH + ROH \ (Hydrolysis) \quad (Eq4)$$

Sol-gel shelf-life was recorded to be less than three months; due to the progression of the reactions in Equations 2-4. The literature was reviewed and consulted to survey working and optimal PZT sol-gel preparations that might reveal the reasons for the inferior results obtained with the Starting Formulation of this work.

6.1.2 MODIFIED PZT FORMULATION

The PZT sol-gel was modified to avert concerns with incomplete hydrolysis as well as to lower the viscosity of the ink to permit printing. According to Yao et al., by implementing a polymer to the additive package, such as polyethylene glycol (PEG), it would aid in film formation and inhibit cracking upon sintering.[32] This is because a large polymer has a high boiling point. It will not evaporate at low temperatures and will rather slowly leave the PZT film over the course of both the gelation and sintering processes.

The group of Yao, et al., experimented with adjusting the molecular weight of PEG from 400-1200 MW and spin-coated the solution onto platinum substrates.[32] The group found that 1200 MW PEG produced a crack and defect-free ~35 μm thick sol-gel PZT film due to a decrease in residual stress upon thermal annealing. For this work, however, 1200 MW PEG would counteract

the need for a low viscosity ink. From the work of Shuhui, et al., a 600 MW PEG was tested.[33] Using low molecular weight PEG, they reported minimal defects and cracks were found within the deposited films. Multiple depositions were required, however, to obtain the desired film thickness of ~35 μm. Figure 22 shows a thermally sintered PZT (PEG 600 MW) sol-gel spin-coated onto a stainless-steel substrate.
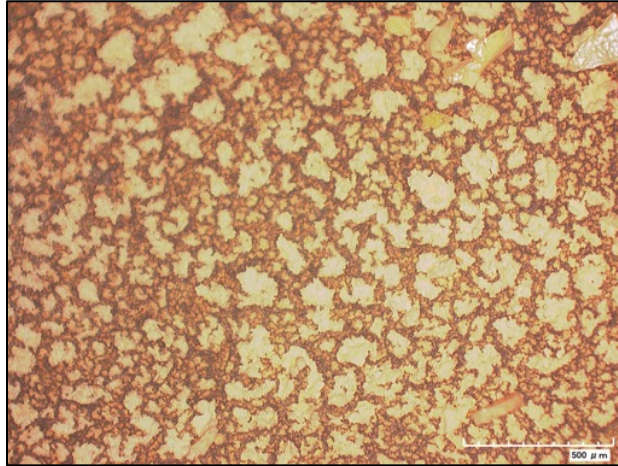
Figure 22. Spin-coated PZT (PEG 600 MW) sol-gel thermally sintered on a stainless-steel substrate (500 μm scale).

Figure 23 shows improvement of PZT grain quality when sintered on a stainless-steel substrate. Although there is cracking between the grains, the magnified image shows no cracking within an individual grain (Figure 23).
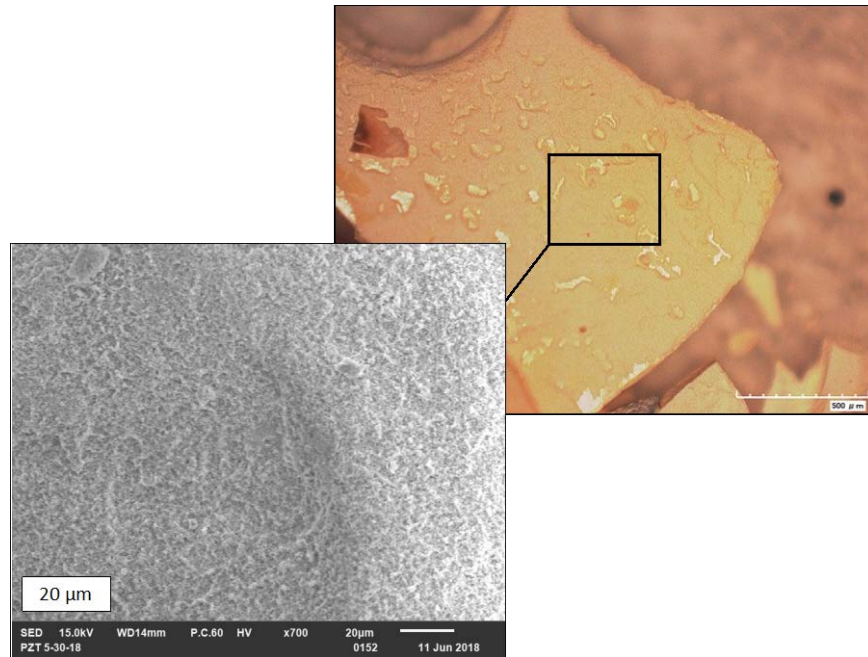
Figure 23. SEM image of delaminated grain of a spin-coated PZT (PEG 600MW) thermally sintered sol-gel on a stainless-steel substrate

The film appeared to be delaminating from the substrate, and this is possibly due to the stress of the grains forming during the sintering process. These results suggested that implementing a polymer to the additive package would help lead towards the development of a defect-free PZT grain.

Qualitative results, though, confirmed that the viscosity of the PZT (PEG 600MW) sol-gel was not in range for that of print deposition. A 200 MW PEG, then, was adapted to this work. The working PEG additive package is shown in Table 4.

Table 4. Modifiied PZT sol-gel fabrication used for NanoJet Printing. Final concentration of composite was 1.6 M.

Compound	Molar Ratio	Sintering Aid	Molar Ratio
Lead Acetate_3H$_2$O	0.50		
Zirconium n-propoxide (Sigma Aldrich)	0.26	Polyethylene Glycol (200MW)	0.36
Titanium n-propoxide (Sigma Aldrich)	0.24		

6.1.3 OPTIMIZED PZT FORMULATION

6.1.3.1 INCOMPLETE CONDENSATION REACTION

Although PEG prevented some cracks forming amongst the grains, defects, such as minimal cracking and pinholes, were still evident in the prints (Figure 24).
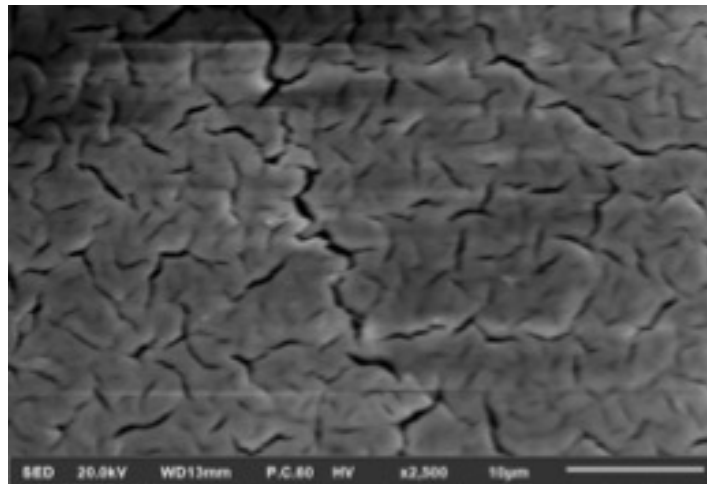
Figure 24. SEM image of spin-coated PZT (PEG 200MW) sol-gel thermally sintered on a stainless-steel substrate (10 µm).

The pinholes and cracks may be related back to the overall sol-gel reaction mechanism. The sol-gel syntheses consist of a series of condensation reactions that occur at the same time, but at

different rates (Eq 3). It was possible that outgassing of volatiles from the products of the condensation reactions was occurring during the sintering of the thin-films.

Under argon gas, the Modified sol-gel PZT composite was heated at 80°C and refluxed for fifteen hours in order for all the reaction processes to reach completion and equilibrium. Upon removal, an acetate film was produced. The acetate film indicated the large number of volatile products present in the sol-gel composite. When removing these products, outgassing and decomposition would no longer cause film defects. These results suggested that all condensation reactions were driven to completion (Figure 25).
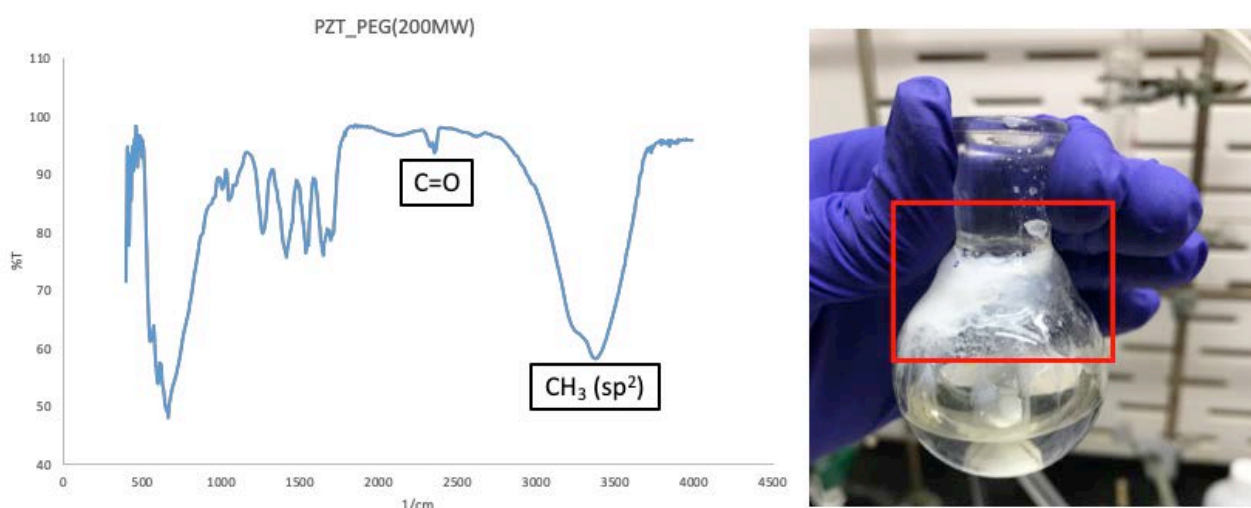
Figure 25. Acetate film infrared (IR) spectroscopy spectra (left) produced after reflux reaction of Modified PZT sol-gel composite (right).

The produced film was characterized using IR spectroscopy and the spectrum was compared to the literature to confirm that the material was an acetate film.[34]

6.1.3.2 OPTIMIZED PZT FORMULATION ADAPTED TO INKJET PRINTING

Inkjet printing, another additive manufacturing printing technique, was adapted to this work alongside with NanoJet printing. Similar to NanoJet printing, inkjet printing requires a specific ink surface and viscosity properties as shown in Table 5.

Table 5. Ink rheology towards an inkjet printable ink.

Viscosity	Surface Tension
1-5 cPs	20-30 dynes/cm

The Modified PZT formulation surface tension was measured to be 16 dynes/cm, which was considered too low for inkjet printing. The surface tension of the ink, therefore, was adjusted by adapting the PZT sol-gel to a pre-determined inkjet printable solution (Table 6).

Table 6. Inkjet printable ink vehicle implemented to PZT sol-gel.

Ink Components	Viscosity	Surface Tension
DI H_2O Propylene Glycol Isopropyl Alcohol	3.6 cPs	30 dynes/cm

The Optimized sol-gel formulation was used for inkjet printing. The newly formulated ink exhibited no precipitation or agglomeration of PZT particles over that time period, confirming that ink was stable. The aqueous-based ink has maintained a shelf-life of over 7 months.

6.1.4 INK CHARACTERIZATION

6.1.4.1 STARTING PZT FORMULATION INK CHARACTERIZATION

The Starting PZT sol-gel formula was analytically characterized using differential scanning calorimetry (DSC)-TGA, XRD and surface tension measurements. According to the DSC-TGA results, the weight percent of the Starting PZT sol-gel was found to be 10% PZT (Figure 26), and the curing temperature needs to be greater than 500 °C. The final concentration of the Starting PZT sol-gel was calculated to be 1.6 M. Typical PZT sol-gel solutions range from 1-1.5M.[28,32,33,35,36]
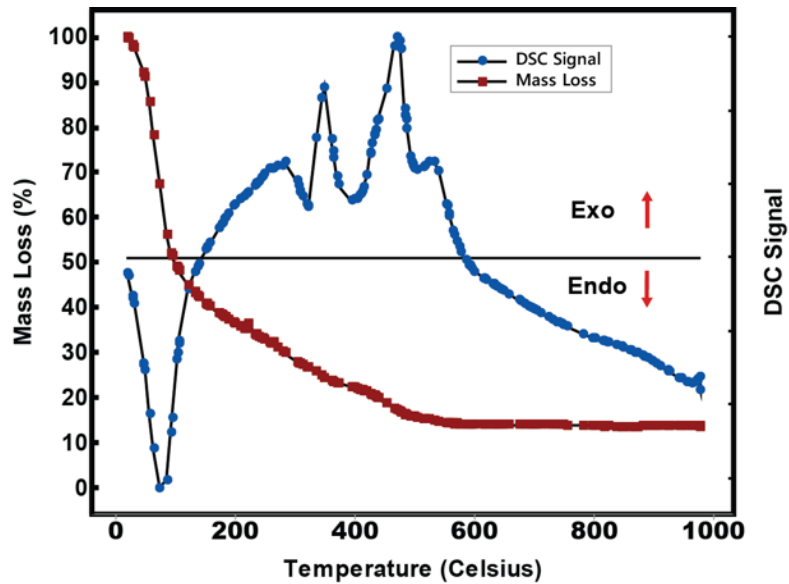
Figure 26. DSC-TGA of starting PZT sol-gel. [35]

A powdered sample of the PZT sol-gel was measured using XRD analysis (Figure 27).
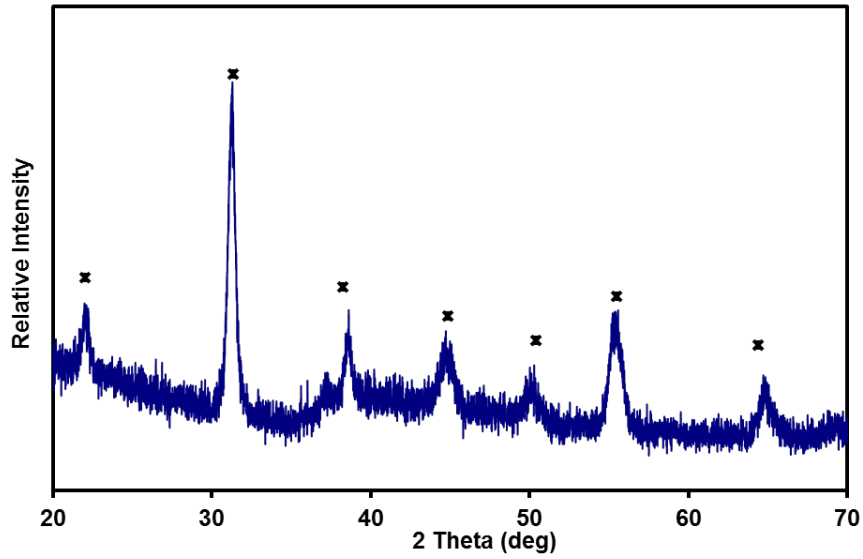
Figure 27. Powder XRD of starting PZT sol-gel. [35]

The XRD confirmed that the perovskite crystal structure of PZT was achieved after thermal sintering. The material, therefore, may exhibit optimal ferroelectric and piezoelectric responses in response to mechanical or electrical properties.

After confirming the concentration and crystal structure of the sol-gel, the surface tension and viscosity of the ink were analyzed. Good print quality is dependent on both surface tension and viscosity of an ink. Both printing methods require a surface tension between 20-30 dynes/cm and an ink viscosity between 1-5 cPs. The surface tension measurements of the PZT sol-gel are compatible with that of both NanoJet and inkjet printing (Table 7).

Table 7. Surface tension measurements of starting PZT formulation.

Ink Formulation	Tip	Average Surface Tension
Starting PZT Formulation	Teflon	22.39 dynes/cm

The Starting ink viscosity was estimated to be too high for optimal print deposition based on the flow behavior.

6.1.4.2 MODIFIED & OPTIMIZED PZT FORMULATION INK CHARACTERIZATION

The Modified and Optimized PZT sol-gel was analytically characterized using TGA and surface tension measurements. According to the TGA results, the weight percent of the Modified PZT sol-gel was found to be 10%, similar to that of the Starting PZT sol-gel (Figure 28). There were two thermal decomposition temperatures for Modified PZT around 300 °C and 600 °C. The 300 °C may correspond with PEG decomposition while 600 °C was PZT formation. Since the PEG has a large molecular weight, the mass loss of the polymer occurs slowly as the temperature increases.
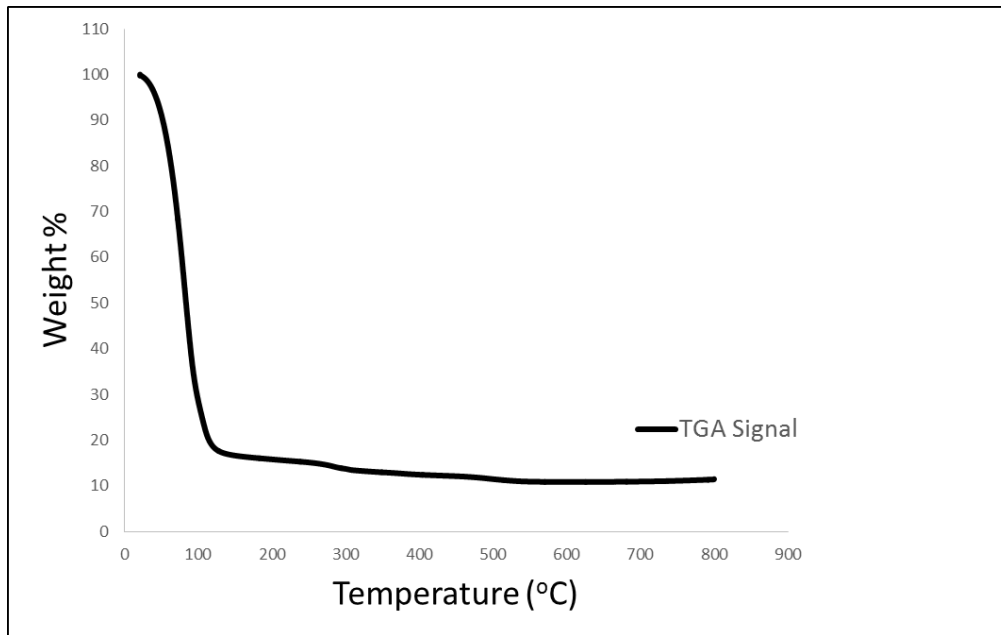
Figure 28. TGA of Modified PZT sol-gel.

A TGA of the Optimized PZT sol-gel yielded a weight percent of PZT of 5% (Figure 29). The curing temperature range of the sol-gel was found to be around 200 ºC and 300 ºC. Rich with oxygen functionality, the ink jet vehicle component addition appears to lower the PZT sintering temperature by 300 ºC. More analysis would be required, but if this result is found to be reproducible, a 300 ºC sintering temperature would be a substantial process improvement.
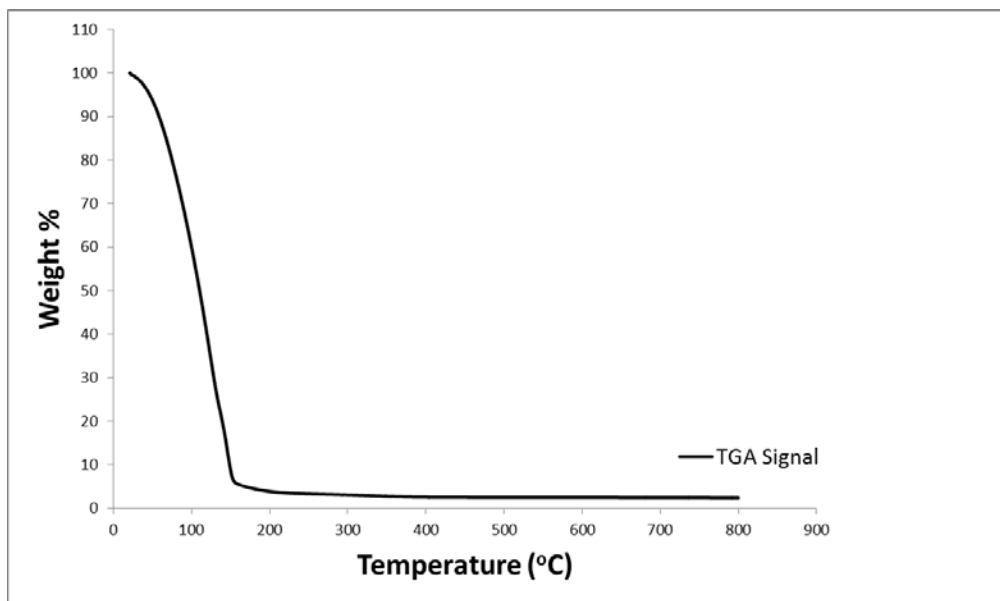
Figure 29. TGA of Optimized PZT sol-gel.

The surface tension and viscosity were measured of the Modified and Optimized PZT sol-gel. The surface tension measurement of the Optimized sol-gel was considered within the working range for both NanoJet and inkjet printing methods (Table 8).

Table 8. Surface tension measurements of modified PZT formulation.

Ink Formulation	Tip	Average Surface Tension
Modified PZT Formulation	Teflon	16 dynes/cm
Optimized PZT Formulation	Teflon	30 dynes/cm

Based off qualitative results, the viscosity of the ink was also optimal for both printing methods.

6.2 PZT PRINT DEPOSITION

6.2.1 SUBSTRATE SELECTION

Quartz and stainless-steel are both chemically compatible materials with PZT. Given stainless-steel is a conductive substrate, it provides the opportunity to develop a working device, potentially requiring less fabrication costs over rare metal films (Figure 30).
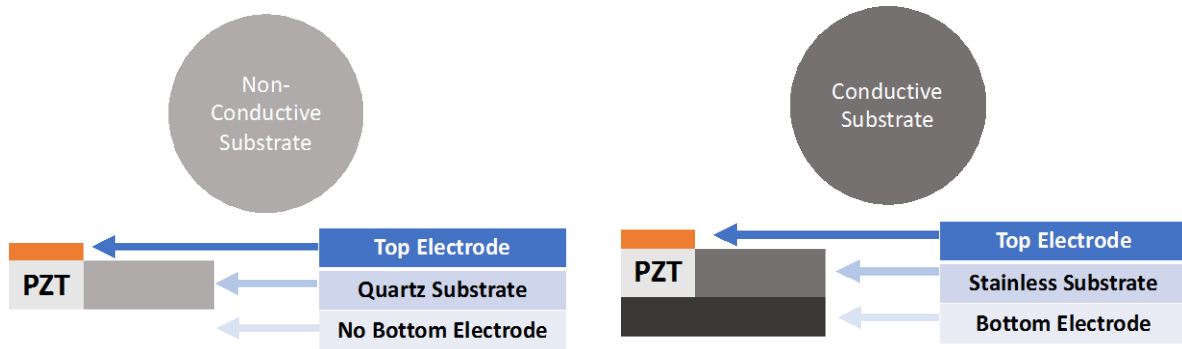
Figure 30. Schematic of a non-working device compared to a working device.

A non-conductive substrate, shown in Figure 30, indicates that the material does not have a bottom electrode. Adding connections to the material via gold sputter coating techniques, would fabricate a bottom electrode on the quartz (Figure 31).
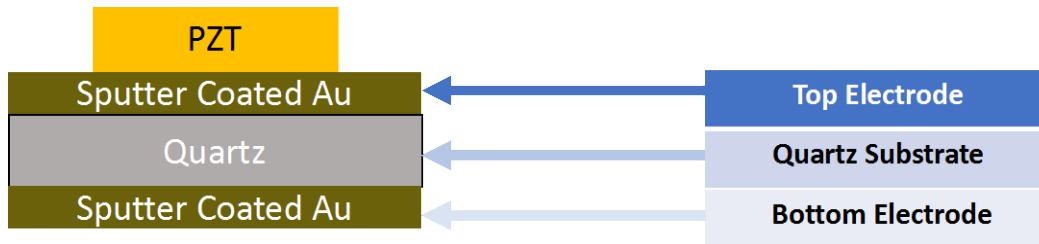
Figure 31. Schematic of functionally grading quartz with sputter coated gold.

The functional graded material technique, and implementing gold on the substrate, is both costly and hinders the fast throughput process. Using an inexpensive metal, such as stainless-steel, allows the project the opportunity to adapt to large-scale manufacturing methods.

Various stainless-steel substrates, therefore, were investigated for this work. Stainless-steel flexible foils and polished stainless-steel substrates were used in conjunction with the modified

PZT formulation. The stainless-steel foil was an interesting substrate to adapt to this work because it would potentially move the project into the developing field of printed electronics.

6.2.2 STARTING PZT FORMULATION

6.2.2.1 NANOJET PRINTING

According to Integrated Deposition Solutions, Inc (IDS), film deposition of an ink will require low sheath flow, and relatively high aerosol flow; depending on desired thickness of film.[37] The atomizer unit should also maintain a current flow of 0.42 amps. The viscosity of the ink should range between 1-5 cPs. This range permits aerosol droplet formation of the ink based on the suggested current flow from the atomizer unit.[37]

Although the viscosity of the ink was known to not fall within the working print parameters of NanoJet printing, preliminary prints were still trialed. Aerosol production and print deposition of the Starting PZT sol-gel was not attained from the suggested parameters from IDS. High viscosity, outside the recommended range, was the suspected cause. Rather than modifying the ink composition, the printing parameters were adjusted. Printing parameters, as shown in Table 9, were found to achieve a printed trace (see Figure 32).
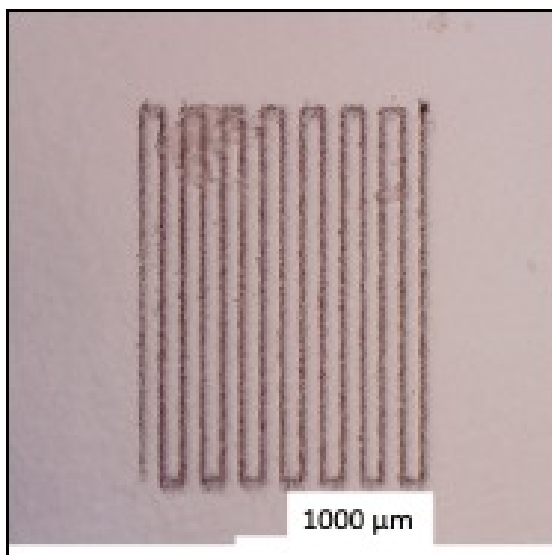
Figure 32. NanoJet printed 200 μm trace width serpentine of Starting PZT sol-gel on stainless-steel substrate.

Theoretically, by increasing the current flow of the atomizer unit, the number of ultrasonic waves transmitted to the ink reservoir would increase, and in turn produce more aerosol droplets.

Table 9. Print parameters used for serpentine depositions of PZT sol-gel on stainless-steel substrate.

Ink Formulation	Aerosol Flow (sccm)	Sheath Flow (sccm)	Atomizer Unit (A)	Print Speed	Nozzle Gauge	Standoff Distance
Starting PZT Formulation	60	50	0.54	2.0 mm/s	22	2.0 mm

Since ink deposition was achieved using the print parameters found in Table 9, the same parameters were trialed in attempts to achieve film deposition (Figure 33).
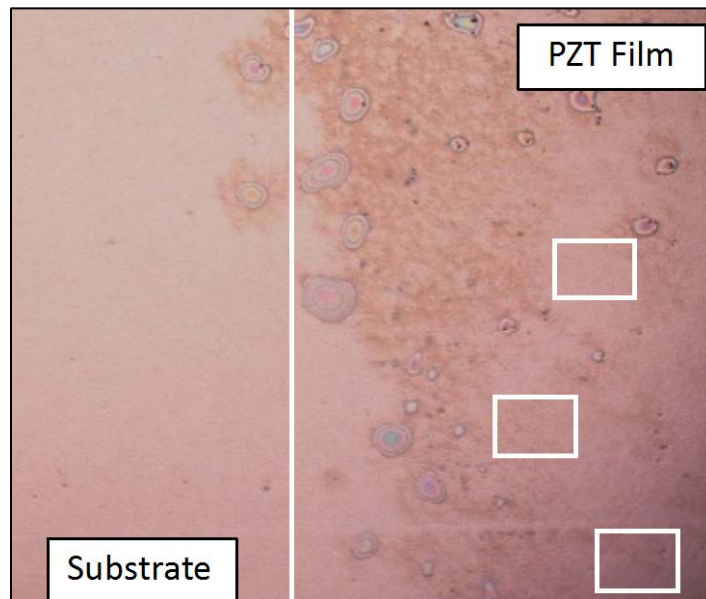
Figure 33. NanoJet printed one centimeter square of Starting PZT sol-gel on stainless-steel substrate. White boxed regions show areas in which film was not infilled. (500μm).

The print shown in Figure 33 indicated that the amount of aerosol droplets formed and deposited did not create an infilled film. The flow rate of both aerosol and sheath, therefore, were adjusted to increase amount of aerosol droplets directed to the deposition head and decrease fine line printing (Table 10).

Table 10. Print parameters used for film depositions of PZT sol-gel on stainless-steel substrate.

Ink Formulation	Aerosol Flow (sccm)	Sheath Flow (sccm)	Atomizer Unit (A)	Print Speed	Nozzle Guage
Starting PZT Formulation	90	40	0.54	2.0 mm/s	22

The new print parameters were used to develop the film shown in Figure 34.
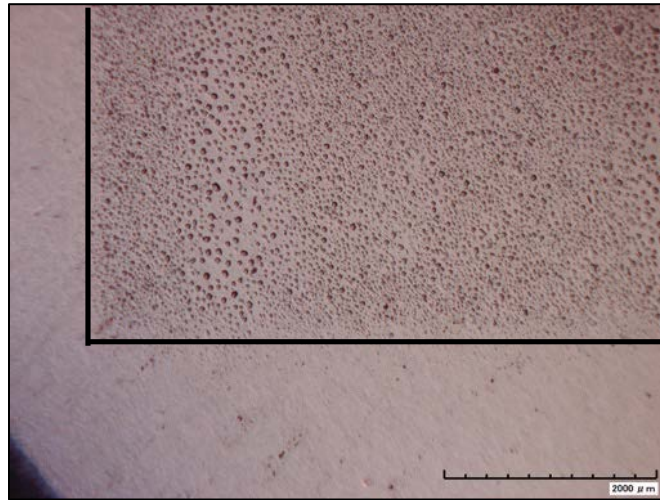
Figure 34. NanoJet printed one cm square of Starting PZT sol-gel on stainless-steel substrate (2000µm).

Film deposition was enhanced when increasing the amount of aerosol droplets deposited on the substrate. Using this method, however, would decrease lifetime of atomizer unit and digital transducer. Prior to deposition of the PZT sol-gel, the digital transducer was replaced. After increasing the atomizer current flow past the manufacturing suggested limits, the digital transducer was found to only perform for three months. Since lifetime of the transducer decreased, the ink was modified in respect to the printing technique.

6.2.3 MODIFIED PZT FORMULATION

6.2.3.1 NANOJET PRINTING

The ink rheology, shown in Table 1, of the Modified PZT sol-gel was considered to be NanoJet printable. For thin-film deposition low aerosol flow, slow print speed, and 0.42 amps set on the atomizer unit were suggested factors for a NanoJet printable ink. The working print parameters for the Modified PZT sol-gel, though, required relatively high aerosol and high current flow (Table 11).

Table 11. Print parameters used for film depositions of Modified PZT sol-gel on stainless-steel substrate.

Ink Formulation	Aerosol Flow (sccm)	Sheath Flow (sccm)	Atomizer Unit (A)	Print Speed	Nozzle Gauge	Standoff Distance
Modified PZT Formulation	80	80	0.51	2.0 mm/s	22	2.0 mm

The aerosol and current flow were set to these values in response to the realization that the ink was adhering to the walls and baffle of the flow cell. The flow cell and baffle are both made up of aluminum. Aluminum has a surface energy of 850 dynes/cm.[38] From the large difference in surface energy between the aluminum surface and the Modified ink, the PZT aerosol droplets adhered to the walls of the flow cell, preventing print flow. The current flow was then increased to produce more aerosol droplets in the ink reservoir. As well, the aerosol flow was increased to carry these aerosol droplets to the deposition head. By increasing the amount of aerosol droplets formed and the aerosol stream carried to the deposition head, the loss of PZT remaining on the walls of the flow cell was counteracted.

The PZT sol-gel was NanoJet printed onto both the polished stainless-steel and stainless-steel foil substrates (see Figure 35). Print quality varied when comparing the Modified PZT sol-gel on both substrates.
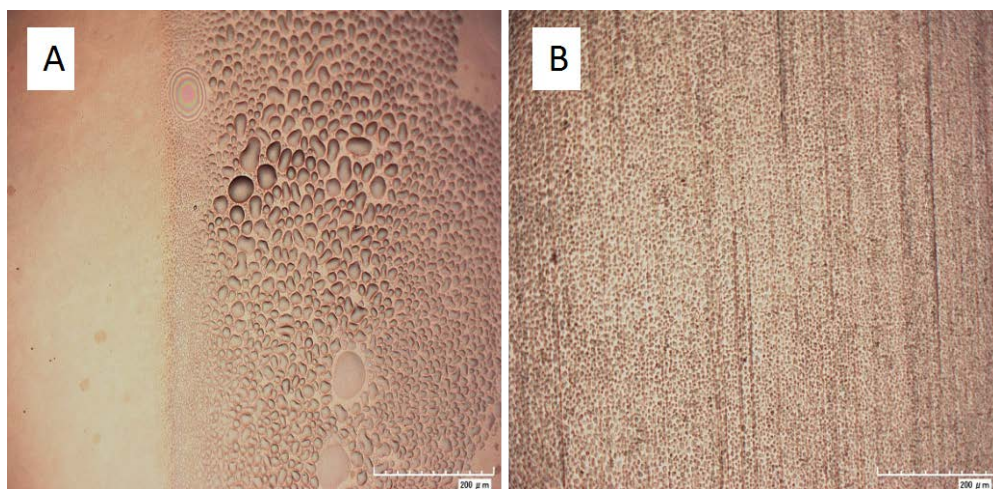
Figure 35. NanoJet printed Modified PZT sol-gel on a polished stainless-steel substrate **(A)** and a stainless-steel foil **(B)** (200µm).

Ink droplet formation ranged in various sizes when PZT was printed on the polished stainless-steel substrate due to the ink crawling back. The Modified PZT sol-gel printed on the stainless-steel foil, however, showed consistent droplet formation and proper film formation.

The observed results can be explained by comparing the surface energy of both substrates as measured by contact angle (Table 12).

Table 12. Contact angle of modified PZT sol-gel on stainless substrates.

Ink Formulation	Substrate	Average Contact Angle
Modified PZT Formulation	Stainless-Steel Foil	28.5 $^\circ$
	Polished Stainless Steel	14.8 $^\circ$

Contact angle illustrates that the change in surface energy between the ink and the polished stainless-steel substrate was smaller than that to the stainless-steel foil. This can be further explained from the Gibbs Free Energy equation, where γ is surface energy.

$$dG = -SdT + VdP \ldots + \gamma dA \text{ (Eq. 4)}$$

When temperature (T) and pressure (P) are constant, the change in free energy, dG, is proportional to the change in surface area, dA, where γ (surface energy) acts as the proportionality constant.

The stainless-steel foil was analyzed using optical profilometry to confirm that the material has a higher surface roughness, and therefore higher surface energy, than the polished stainless-steel substrate (Figure 36).
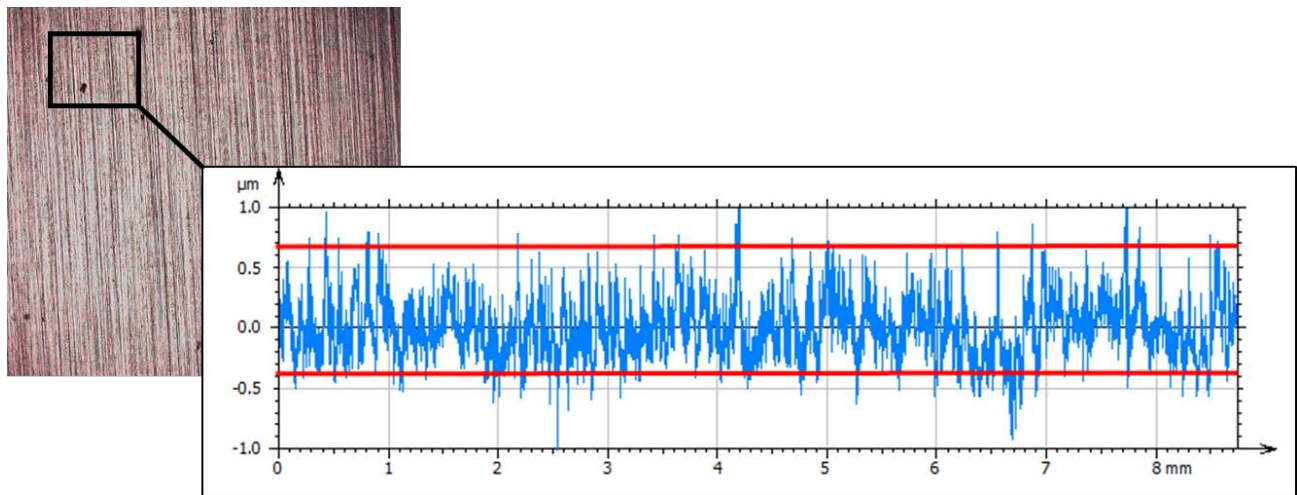
Figure 36. Optical profilometry scan of stainless-steel foil.

Optical profilometry showed that the stainless-steel foil had ± 0.5 μm groves along the substrate and a measured surface roughness of 0.141μm.

A polished stainless-steel was also characterized using optical profilometry (Figure 37). The profile scan of the polished stainless-steel shows minimal groves along the surface and measured a surface roughness of 0.124 μm. The overall surface roughness of the polished substrate, therefore, will be less than that of the foil.
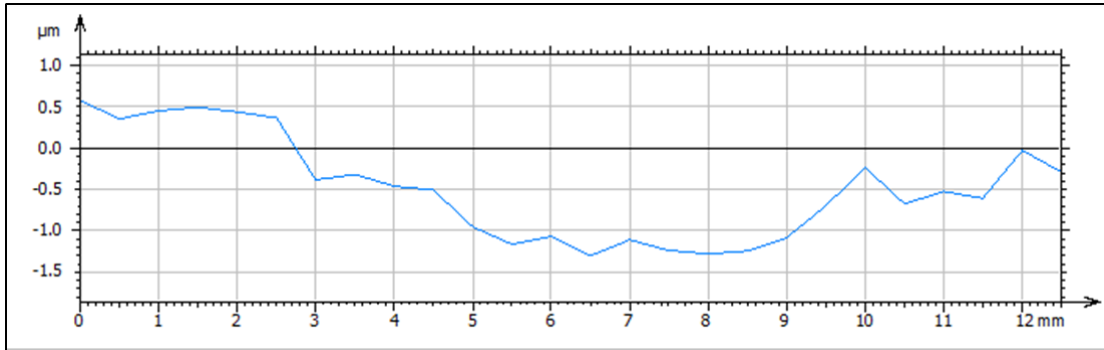
Figure 37. Optical profilometry scan of polished stainless-steel disk.

These results suggest that the stainless-steel foil had a higher surface energy, allowing the Modified PZT sol-gel to experience proper adhesion upon deposition.

Using polarized optical microscopy (see Figure 38), supports the optical profilometry measurements.
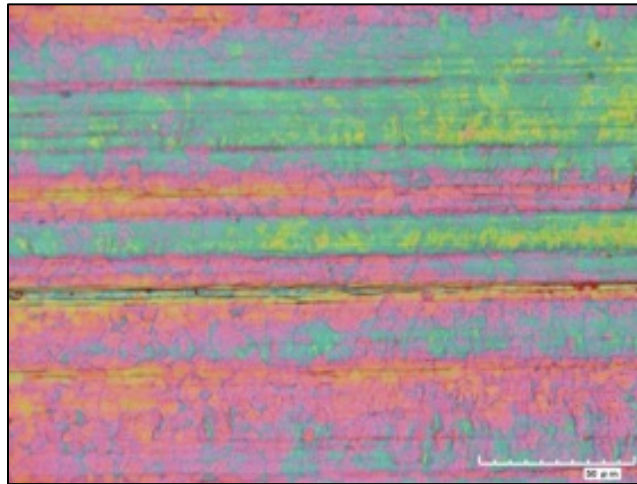
Figure 38. Polarized optical imaging of the modified PZT sol-gel deposited on stainless steel foil (50 μm scale).

The multiple colors imaged from the film, under polarized light, indicated that the film was comprised of multiple thicknesses, and ultimately non-homogenous.

6.2.3.1.1 SUBSTRATE CLEANING

Since the stainless-steel foil was found not to be a suitable substrate, the polished stainless-steel substrate underwent surface treatment to enhance ink adhesion. A cleaning method, using 1.8 M nitric acid was used (Figure 39).
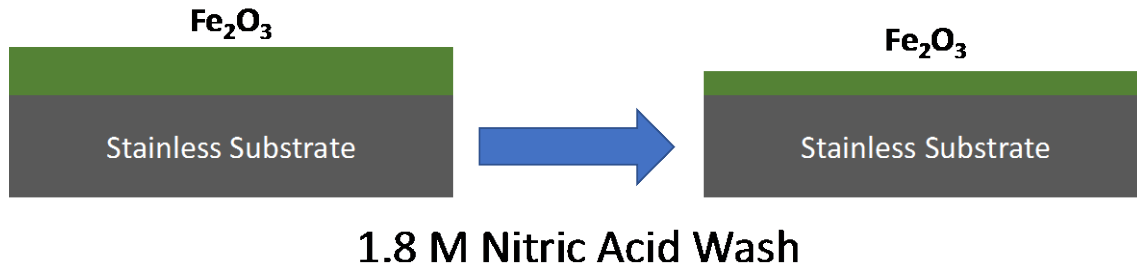
Figure 39. Schematic depiction of acid treatment.

The cleaning method acts as an oxide etching treatment. By partially removing the native oxide layer, found on stainless-steel substrates, the surface energy of the substrate would decrease. A decrease surface energy would result in an increase in the measured contact angle of the deposited Modified and Optimized PZT sol-gel (Table 13).

Table 13. Contact angle measurements of the modified PZT sol-gel on polished stainless-steel before and after nitric acid wash. Measurements were compared to an untreated stainless-steel foil.

Substrate	Before Treatment	After Treatment
Polished Stainless-Steel	14.81º	21.21º
Stainless-Steel Foil	28.50º	

Figure 40 shows the modified PZT sol-gel NanoJet printed onto a stainless substrate after cleaning.
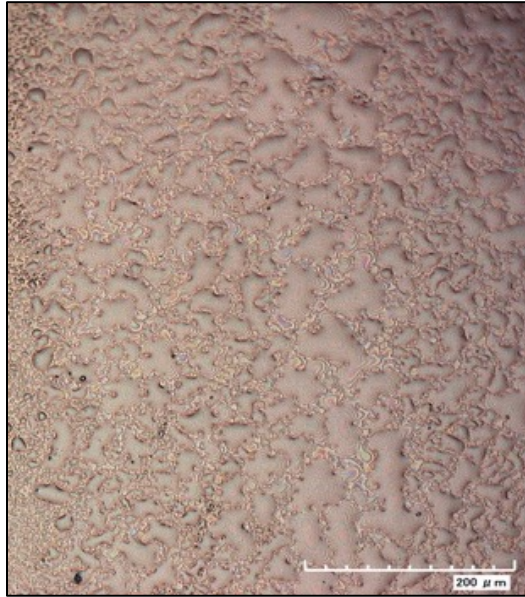
Figure 40. NanoJet printed PZT sol-gel (200 μm scale).

The ink deposition and film quality showed improvements from that shown in Figure 33. Although the wet film formation was still not homogenous, the ink and substrate wetting improved. Better wetting resulted from a substrate surface energy decrease after acid treatment. The film quality would not lead to a uniform film thickness upon thermal sintering either. While the ink was atomized in the ink reservoir, an increase in thermal energy occurred in response to the ultrasonic waves produced to atomize the sol-gel. Some gelation may have occurred from the ultrasonic heating with a corresponding increase in viscosity. Changing viscosity would result in changing print quality. Since the NanoJet printing performance is so dependent on ink rheology, more research would need to be done to inhibit gelation processes that affect print quality.

6.2.3.2 INKJET PRINTING

The Optimized PZT sol-gel ink (Chapter 5, Section 3.3) was then applied using inkjet printing. The printing parameters that produced stable ink jet droplets are shown in Table 14. The waveform voltage used for printing was pre-determined based on the inkjet ink that was adapted to this work.[20] The temperature of each ink cartridge stayed at room temperature in order to prevent the PZT sol-gel from undergoing a gelation process.

Table 14. Print parameters used for film depositions of PZT sol-gel on stainless-steel substrate.

Ink Formulation	Waveform	Standoff Distance	Platen Temperature	Cartridge Temperature
Optimized PZT Formulation	24 V	1250 μm	25 ºC	25 ºC

The wet PZT film printed using nitric acid cleaned stainless steel is shown in Figure 41.

Figure 41. One cm square, inkjet printed Optimized PZT sol-gel on a polished stainless-steel substrate (500 μm scale).

The rheological properties of the Optimized PZT ink were adjusted to be in working range of inkjet printing parameters. The increase in surface tension led to better adhesion of the Optimized PZT on the substrate, enhancing the as-printed film quality.

6.3 PZT POST PROCESSING

Sol-gel films post-processing entails curing and sintering steps. Sintering involves atomic diffusion from one location to another. Prior to this step, the sol-gel underwent a curing process to allow the film to go through the gelation route in the sol-gel mechanism. The gelation process occurs from the condensation reactions that are associated with the sol-gel synthesis. Once the solution has become a gel, sintering is then conducted. During the sintering process, the material will form a metal oxide film, and all volatiles that may have remained in the gel, such as gel forming and sintering aids, will be evaporated off.

Curing and sintering conditions of the PZT films printing using the Modified formulation were optimized in this project. The Starting PZT sol-gel would cure at room temperature for several hours in ambient conditions. This curing method was optimized, for the Modified formulation, by thermally heating the sample via a hotplate or near infrared (NIR) lamp. Both methods involved heating the deposited film on the polished stainless-steel substrate at a range of 80-100 ^{o}C for 15 minutes. The parameters, therefore, were set to use an Adphos NIR lamp for 15 minutes at 90 ^{o}C. This method limits substrate heating, being that it is a top-down thermally curing approach, rather than a bottom-up approach like hot-plate heating. Defect-free gel formation may result since thermal expansion of the substrate has been limited. NIR lamp produced superior results over a hotplate.

Thermal sintering in a muffle furnace is a commonly practiced technique. Optimizing thermal sintering of PZT films, in a muffle furnace, was performed. At the start of this project, the sintering parameters consisted of the film being sintered to 800 ^{o}C at a ramp up rate of 25 ^{o}C/minute.

A temperature of 800 ºC was maintained for approximately an hour, then the film was slow cooled at a rate of 25 ºC/minute to 25 ºC (Figure 42).
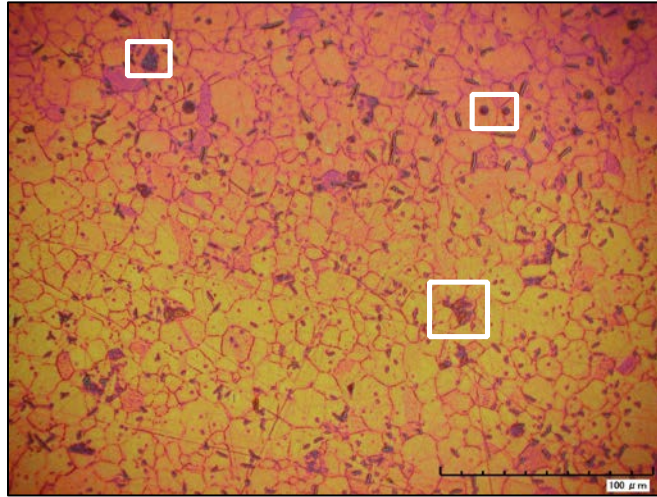
Figure 42. Optical image of a deposited starting PZT sol-gel film on a polished stainless-steel substrate. Examples of defects and cracks are highlighted (100 μm scale).

The produced PZT films presented various defects and cracks within the grains (Figure 42). This confirmed that the thermal sintering method needed to be adjusted.

6.3.1 MODIFIED PZT FILM SINTERING

According to the group of Shuihu et al., when implementing high molecular weight PEG to the PZT sol-gel additive package, a crack and defect-free thick film was produced with spin-coated samples.[33] These crack and defect-free films were produced using a rapid heat up and slow cool down process. The rheological properties between the Modified PZT sol-gel and Shuihu group's sol-gel differ from one another. Deposition of the sol-gels and film thickness were other variant factors. The sintering method from the Shuihu group, though, was implemented to gather preliminary sintering information to better understand the role PEG has in the sol-gel.

Figure 43 shows a thermally sintered film in a muffle furnace. The sample was cured using an AdphosNear-IR lamp at 90 ºC for 15 minutes. The film was heated from 25 ºC to 700 ºC at a rate of 100 ºC/minute. After one minute, upon reaching 700 ºC, a slow cool down process followed. The PZT film was cooled to 25 ºC at a rate of 50 ºC/minute.

The SEM image of the rapidly heated and slow cooled PZT film displayed random cracks along the PZT grains, as highlighted in outlined boxes of Figure 43.
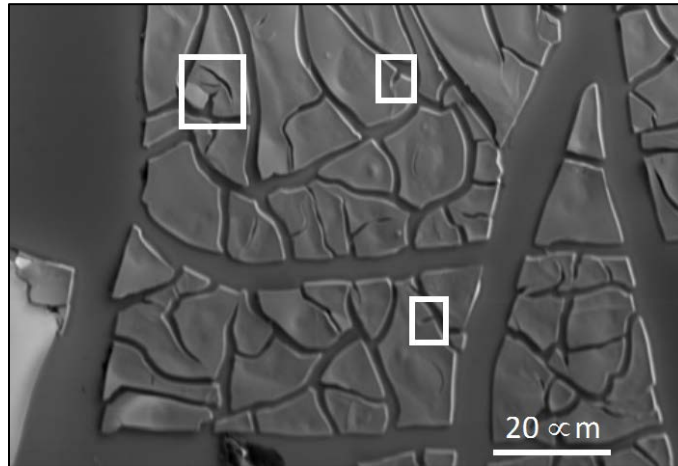
Figure 43. SEM image of a NanoJet deposited Modified PZT sol-gel film on a polished stainless-steel substrate.

These cracks indicated defects within the film. As mentioned previously, the rate at which stainless steel expands is greater than that of PZT. The rapid heat up process was meant to introduce the stainless-steel to thermal energy for a shorter amount of time, to inhibit the material from expanding. The slow cool down process, however, still introduced a change in thermal energy to the stainless-steel substrate over a longer period of time. The stainless-steel substrate, therefore, was undergoing both thermal expansion at elevated temperatures, and thermal compression at lower temperatures. Cracks and defects in the PZT, consequently, were caused by the substrate expanding and compressing. From these observations, it was understood that the substrate needed to be minimally exposed to thermal energy.

The work of Wang et al., studied a slow heat up process and a rapid cool down process of a ceramic material.[39] Understanding that optimal PZT film sintering would be aided by decreasing the amount of time that the substrate was heated, the Wang method was adapted to the sintering process used for the Modified PZT sol-gel.[39]

Figure 44 shows a PZT film that was deposited on a stainless-streel substrate and sintered in a muffle furnace. The sample was cured, prior to sintering, using an Adphos NIR lamp at 90 °C for 15 minutes. Upon curing the PZT, the sample was heated to 700 °C at a ramp up rate of 100 °C/minute. The PZT film incubated at 700 °C for one minute and was immediately removed from the furnace to room temperature.
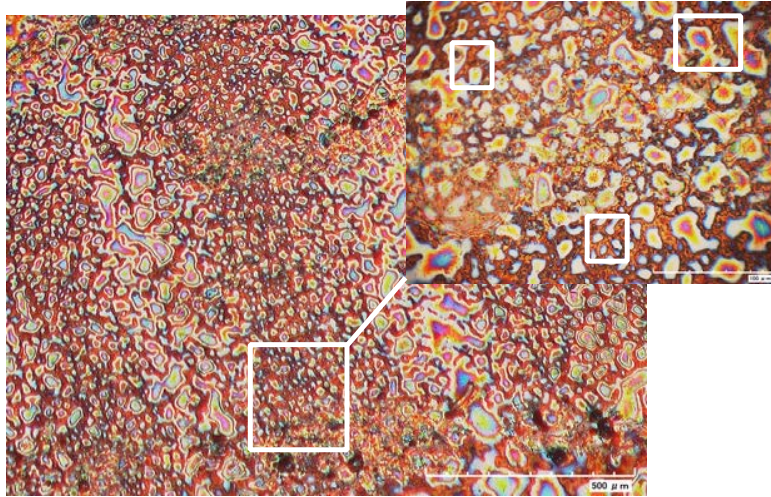
Figure 44. Optical image of a NanoJet deposited Modified PZT sol-gel film on a polished stainless-steel substrate post thermal sintering (500 μm scale).

In Figure 44, examples of defects and cracks are highlighted in the boxed areas. The rate at which both the substrate and sintered film would expand occurred so quickly, due to the rapid heat up technique, that when removed from the furnace the materials would rapidly compress, due to the drastic change in temperature from 700 °C to 25 °C. Significant cracking and defect formation were an outcomes of this sintering method.

6.3.2 RAPID CYCLE PZT FILM SINTERING

Additive manufacturing and large-scale manufacturing were key motivating models for this work. Scalability for fabricated working devices, was kept in mind when adjusting post-processing of the film. The rapid heating and cooling method, was modified to develop a sintering process that adapts to large-scale manufacturing.

Linde's U.S. additive manufacturing group produced sintered metal powder films from a rapid cool down approach by introducing liquid nitrogen to the material.[40] Using the determined Optimal sol-gel formulation, the liquid nitrogen approach was adapted to the rapid sintering

method. Quenching both the substrate and ceramic film in liquid nitrogen would hinder negative effects of slow thermal cooling. Substrate thermal expansion could be effectively minimized, preventing film defect formation. Rapidly freezing the materials, quenched in liquid nitrogen, could eliminate the negative effects of thermal expansion. Combining both ideas enhanced the opportunity to fabricate a fully sintered crack and defect-free PZT film.

The inkjet deposited PZT film, on a stainless-steel substrate, shown in Figure 45 had been cured using an Adphos NIR lamp for 90 ^{o}C for 15 minutes.
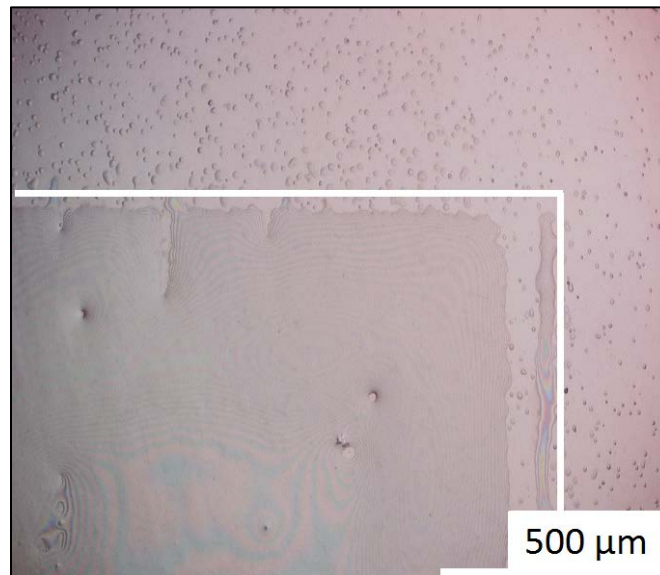
Figure 45. Optical image of a nearly defect free inkjet deposited modified PZT film on a polished stainless-steel substrate.

The film was sintered to 700 ºC at a ramp up rate of 100 ºC/minute. The material remained at 700 ºC for one minute. The PZT film was then quenched in liquid nitrogen. An example of a sintered PZT film from this adapted method can be seen in Figure 46.
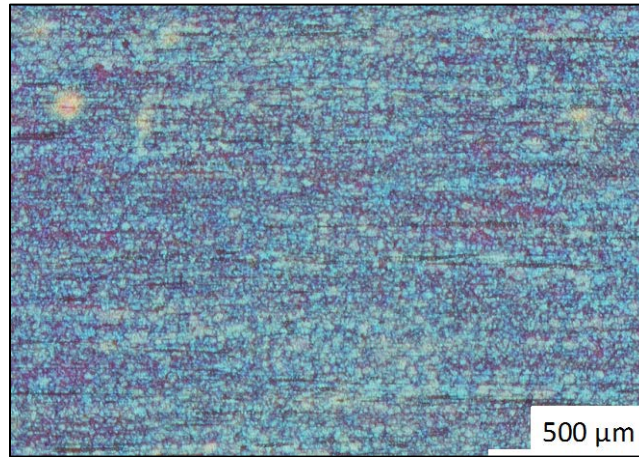
Figure 46. Polarized optical image of an inkjet deposited modified PZT sol-gel film on a polished stainless-steel substrate.

Figure 46 demonstrates a crack and defect-free PZT thin-film. The polarized optical image shows that the film was homogenous. The material exhibited no cracks and defects; meaning that the material will not short in device applications. Under polarized light, the blue image indicates both a thin film, on the order of 0.4-0.5 µm, and homogeneous in thickness. The optical image does reveal evidence of cracking or defects across the film surface.

This sintering method enabled the production of multiple crack and defect-free films. Some examples of these films can be seen in the SEM images found in Figure 47.
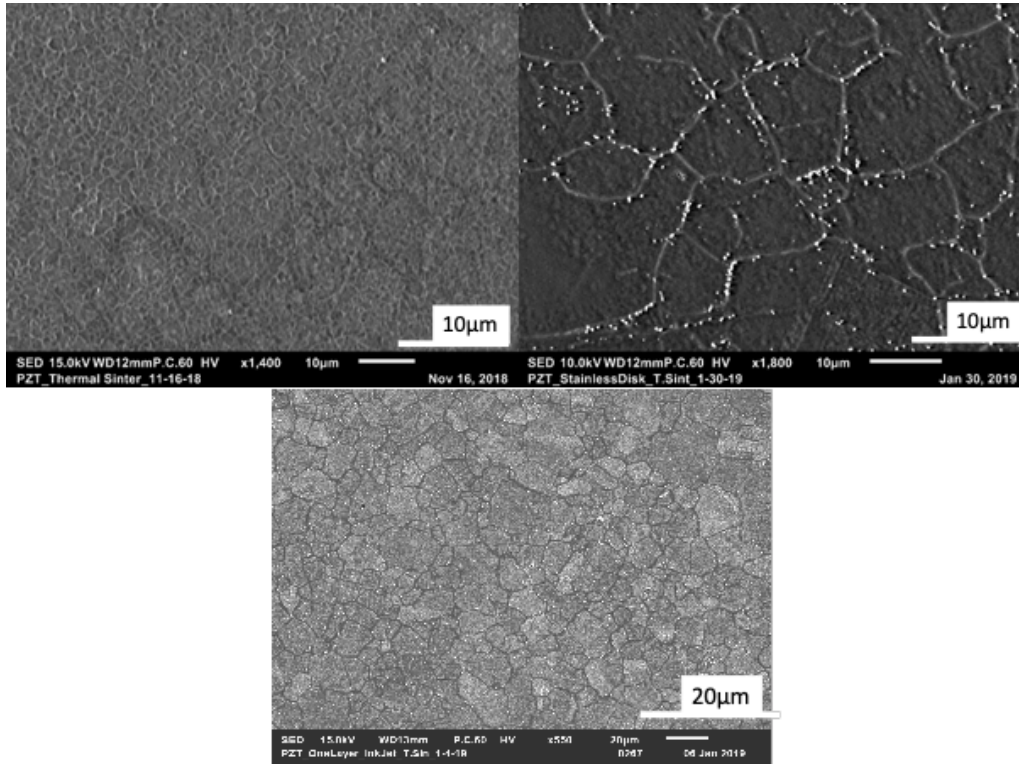
Figure 47. SEM imaging of examples of crack and defect-free sintered PZT thin-films.

In the SEM images above, white particles were found between the PZT grain boundaries. These are lead oxide particles, which was confirmed through EDS analysis. Lead oxide is formed during the sintering process. Rather than the PZT film experiencing a loss of lead from the composite, the produced lead oxide was forming between the individual grains. The dense grain boundaries have a larger surface area than that of the grains themselves, therefore the grain boundaries have a larger surface energy. The larger surface energy then, in turn, causes the nucleation sites for chemical processes, such as lead oxide growth, during the sintering process. When the film was not sintered optimally, random cracking will occur amongst the PZT grain boundaries. However, proper sintering of the film will cause the excess lead oxide to form amongst these grain boundaries and act as a sintering aid to the PZT grain crystal structure.

6.3.2.1 SINTERED PZT FILM CHARACTERIZATION

6.3.2.1.1 ENERGY-DISPERSIVE X-RAY SPECTROSCOPY ANALYSIS

The sintered film composition was evaluated using SEM-EDS analysis (see Table 15). To confirm the excess lead material, and the formation of the Zr/Ti 52/48 ratio, the sintered films were characterized using EDS.

Table 15. EDS results of PZT thermally sintered film.

Substrate	Formula	Mol %	Zr/Ti Molar Ratio %
	PbO	52.53 %	
Polished Stainless-Steel	ZrO_2	25.01%	52.68/47.32
	TiO_2	22.46%	

Based on the EDS results, the PZT film had close to the optimal 52/48 molar Zr/Ti ratio. There was excess lead, which correlates with lead oxide within the grain boundaries.

6.3.2.1.2 RAMAN SPECTROSCOPY

Raman spectroscopy was another analysis method utilized on the thermally sintered PZT thin-film (see Figure 48).
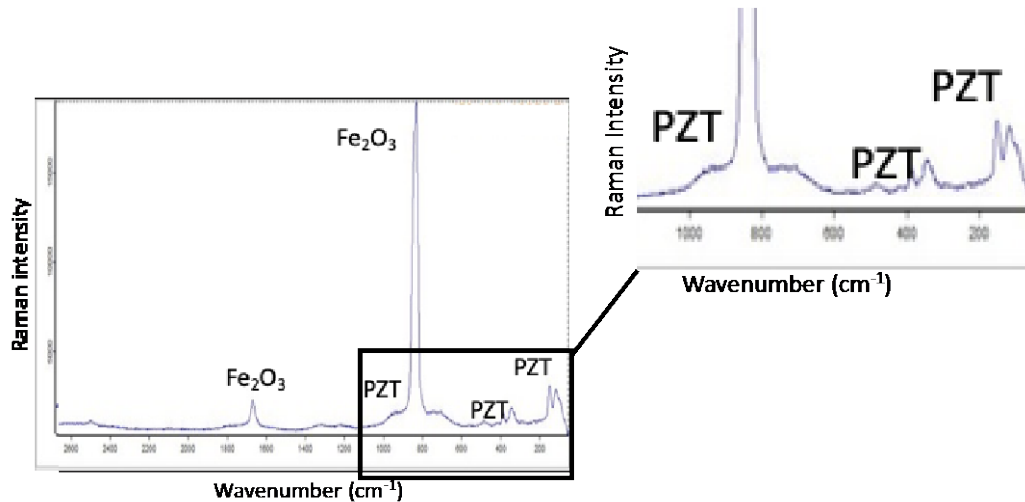
Figure 48. Raman spectra of thermally sintered PZT thin-film on a polished stainless-steel substrate.

The sharp iron oxide (Fe_2O_3) peaks are shown in the Raman spectra because of surface-enhanced effects from the substrate. The measured broad peaks in Figure 48, are PZT peaks, which correlates

to that found in the literature.[41] According to the literature, the Raman spectra of did not show evidence of pyrochlore phase in the sintered PZT film. These results confirmed that the PZT is a fully densified perovskite crystal.[41]

6.3.2.1.3 FERROELECTRIC RESPONSE

The ferroelectric response was measured using a Sawyer-Tower circuit (Figure 49).
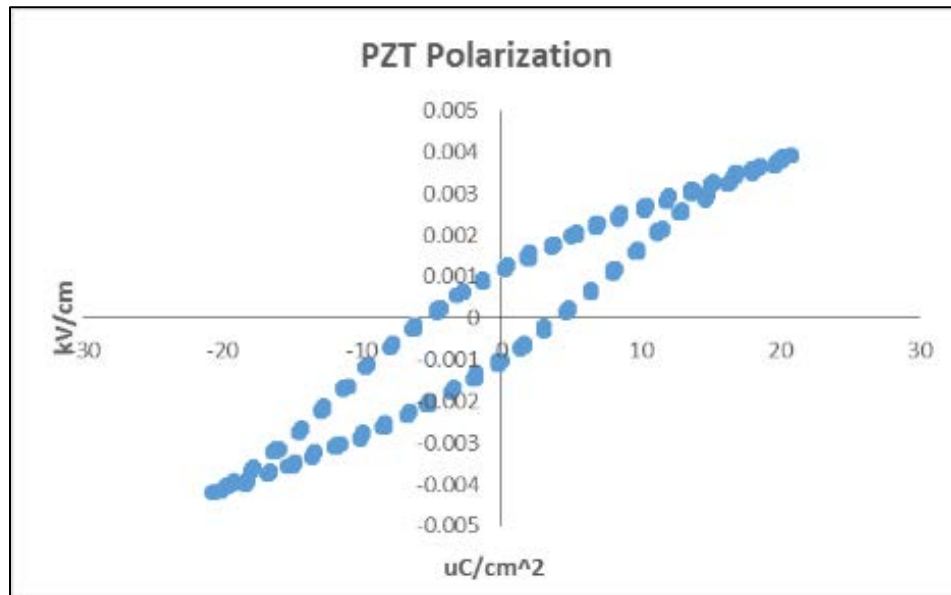
Figure 49. Ferroelectric response of a thermally sintered PZT sub-5 μm film on polished stainless-steel substrate.

The measured samples were unpoled. An unpoled sample, results in the direction of the dipoles to be randomly oriented throughout the grains, potentially leading to a weaker ferroelectric response relative to a poled sample. A remnant polarization of $\pm$ 0.001 μC/cm^2 was produced.

Although the ferroelectric response from the material was weak, an electrical response from the PZT thin-film was observed when a mechanical force was applied to the substrate. When tapping the substrate, a measureable electrical response on an oscilloscope was detected. In order to optimize the ferroelectric response from the PZT film, a better top electrode must be fabricated for the device. This work utilized copper tape as the top working electrode. Poor adhesion of the copper tape on the PZT film led to a weak connection between the film and top electrode, which in turn led to a weak ferroelectric response from the PZT film. This qualitative analysis confirmed

that a PZT sol-gel was formulated and deposited using additive manufacturing techniques and rapidly sintered into a crack and defect-free thin-film to create a working device.

CHAPTER SEVEN- SUMMARY

A novel PZT sol-gel synthesis was developed. The sol-gel comprised of an alkoxide mixture with a Zr/Ti ratio of 52/48. The polymer, PEG (200 MW), was realized to be a superior film forming and thermal sintering aid. The PEG containing PZT sol-gel was adapted to two additive manufacturing processing techniques, NanoJet and inkjet printing. NanoJet printing was performed with the Modified PZT sol-gel formulation yielding a non-homogenous thin-film. Thick-film deposition of the Modified PZT sol-gel may be possible using a build-up deposition approach. Print quality was optimized when the Optimized PZT sol-gel was adapted to inkjet printing. Reproducible PZT thin-films were achieved after inkjet deposition, curing and sintering were completed.

Crack and defect-free film sintering was successful using a rapid thermal sintering approach. The PZT film was sintered for 700 $^{\circ}$C for one minute before being quenched in liquid nitrogen. This method hindered the process of thermal expansion between the chosen stainless substrate and the deposited PZT ceramic material. This newly adapted thermal sintering method may permit high throughput manufacturing.

The PZT films were characterized using Raman spectroscopy, SEM-EDS, and ferroelectric response measurements. EDS results showed that the PZT consisted of the proper 52/48 Zr/Ti molar ratio. This molar ratio was confirmed by Raman spectroscopy. There was no evidence of a pyrochlore PZT phase in the spectra. EDS and Raman spectra suggested that the material may exhibit a ferroelectric response. A Sawyer-Tower circuit was used to measure the ferroelectric response of the PZT thin-film. An unpoled sample of PZT measured a remnant polarization of $\pm0.001\mu$C/cm^2. Upon mechanical applied stress, the material exhibited a change in polarization, confirming that the material was a working piezoelectric.

This project demonstrated that a working PZT sol-gel can be fabricated and adapted to additive manufacturing. Rapid thermal sintering proved to be an excellent method when reproducing the PZT films. A working device was developed.

7.1.1 FUTURE WORK

7.1.1.1 DIPOLE MOMENT POLING

PZT has randomly aligned domains. Randomly aligned domains, generally, causes weak ferroelectric responses emitted from the material.[42] This is because when a mechanical stress is applied to the material the dipole vectors are expected to rotate. When the dipoles are in random orientation, the mechanical stress will cause the vectors to rotate into another random orientation. Since the new dipole orientation is still randomized, the expected response will be weak.

To overcome the possibly negligible response, orienting the grains initially upon sintering can be done (Figure 50).
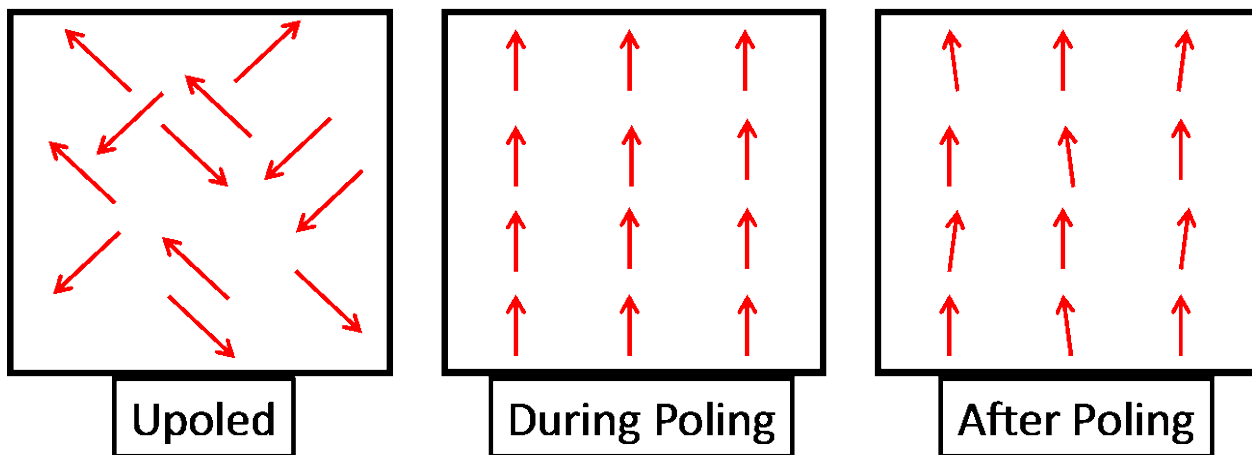
Figure 50. Depiction of an un-poled ceramic material and poled ceramic material. The electric dipole moment vectors are noted by the oriented arrows.

When the material is being poled, a large electric field is applied. Poling causes distortion in the PZT crystal lattice, in response to the applied electric field. The pinning effect causes the dipole vectors to stay relative to the poling direction.[42] Once the poling electric field has been removed from the material, the dipoles are no longer randomly oriented. Orienting the dipoles in the same direction, will then cause for a larger ferroelectric response measured from the material.

According to the work of Ouyang et al., a lower poling electric field was 30 kV/cm.[43] For a film thickness of approximately 5 μm, 15 V should be applied to the material. The poling time suggested in Ouyang et al., work was for two hours. It should be noted, however, that both the time and poling electric field are possibly dependent on the thickness and type of material. Results have been reported of a 100 kV/cm electric field being used over a course of several hours.[43]

7.1.1.1 PHOTONIC SINTERING

Ouyang et al., denoted rapid pulses applied to the sample force film can change crystal phases.[43] Meaning that the material is exposed below and above the Curie temperature. This cyclic temperature digression is reported to simultaneously pol and sinter the PZT film.[43]

Photonic sintering also permits the use of low-temperature substrates. The pulses absorbed by films can last as little as a few microseconds. By implementing the short pulse technique, the film is able to absorb the pulsed flash, rather than the substrate, consequently, limiting substrate heating (Figure 51).

By eliminating substrate heating, concerns regarding thermal expansion rates could be considered insignificant. Low melting point temperature substrates could also be investigated, such as flexible plastic substrates. The thickness of flexible substrates is generally thinner than that of a metallic plate; therefore, the amount of thermal energy that the substrate can be exposed to may change. To confirm the possibility of implementing photonic sintering to this work, the preliminary results of an inkjet deposited PZT sol-gel on the flexible stainless-steel substrate is shared in Figure 51.
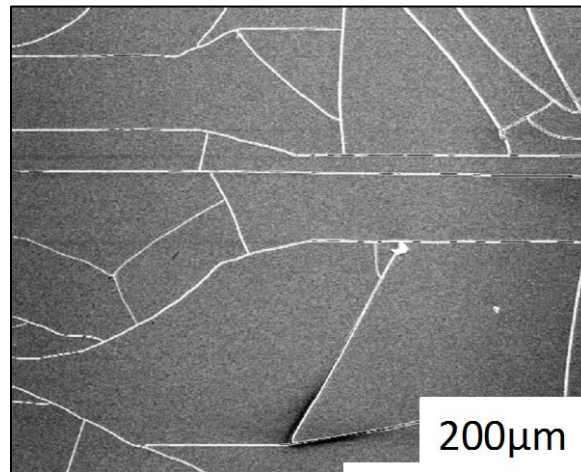
Figure 51. SEM image of a photonically sintered inkjet deposited PZT sol-gel on a stainless-steel foil substrate (200 μm scale).

A 350 μs pulse with a 400 V flash was applied to this film that is shown in Figure 51. Although there was no cracking along the grains, the PZT grains are not fully densified. This can be confirmed on the SEM image scale, for fully densified grains are smaller in size. To enhance grain densification, a larger amount of energy from the flash lamp needs to be exposed to the

substrate. Optimizing the photonic sintering of the PZT sol-gel, would push this project into the field of printed flexible electronics. The field of flexible printed electronics is an innovative discipline of functional printing. Thin-film deposition of an optimal PZT sol-gel onto a flexible, conductive substrate that is rapidly sintered into a crack and defect-free working device will permit a wider range of sensor and actuator applications.

REFERENCES

(1)   Printed electronics Market by Material (Inks and Substrates), Technology (Inkjet, Screen, Gravure, and Flexographic), Device (Sensors, Displays, Batteries, RFID tags, Lighting solutions/panels, and PV Cells), Industry, and Geography - Global Forecast to 2.

(2)   Chung, C.-C. Microstructural Evolution in Lead Zirconate Titanate (PZT) Piezoelectric Ceramics. *Thesis* **2014**.

(3)   Wang, Y. R.; Zheng, J. M.; Ren, G. Y.; Zhang, P. H.; Xu, C. A Flexible Piezoelectric Force Sensor Based on PVDF Fabrics. *Smart Mater. Struct.* **2011**. https://doi.org/10.1088/0964-1726/20/4/045009.

(4)   Marton, P.; Rychetsky, I.; Hlinka, J. Domain Walls of Ferroelectric BaTiO3within the Ginzburg-Landau-Devonshire Phenomenological Model. *Phys. Rev. B - Condens. Matter Mater. Phys.* **2010**. https://doi.org/10.1103/PhysRevB.81.144125.

(5)   Tontonoz, P.; Hu, E.; Graves, R. A.; Budavari, A. I.; Spiegelman, B. M. Iii M .. I . I. **1994**, *4*, 1224–1234.

(6)   W.Schwartz, R. Chemical Solution Deposition of Perovksite Thin Films. *Chem. Mater.* **1997**, *9* (11), 2325–2340.

(7)   Vatansever, D.; Siores, E.; Shah, T. Alternative Resources for Renewable Energy: Piezoelectric and Photovoltaic Smart Structures. In *Global Warming - Impacts and Future Perspectives*; 2012. https://doi.org/10.5772/50570.

(8)   Panda, P. K. Development of PZT Materials, Fabrication and Characterization of Multi Layered Actuators for Aerospace Applications. *AIP Conf. Proc.* **2011**. https://doi.org/10.1063/1.4736880.

(9)   Callister Jr, W. D. Materials Science and Engineering - An Introduction (5th Ed.). *Anti-Corrosion Methods Mater.* **2000**. https://doi.org/10.1108/acmm.2000.12847aae.001.

(10)   Hu, W. Experimental Search for High Curie Temperature Piezoelectric Ceramics with Combinatorial Approaches. **2011**.

(11)   Zhou, Q.; Lau, S.; Wu, D.; Kirk Shung, K. Piezoelectric Films for High Frequency Ultrasonic Transducers in Biomedical Applications. *Prog. Mater. Sci.* **2011**. https://doi.org/10.1016/j.pmatsci.2010.09.001.

(12)   Kobayashi, T.; Maeda, R. Piezoelectric Optical Micro Scanner with Built-in Torsion Sensors. *Japanese J. Appl. Physics, Part 1 Regul. Pap. Short Notes Rev. Pap.* **2007**. https://doi.org/10.1143/JJAP.46.2781.

(13)   Simon, S. H. (Oxford U. Solid State Basics. *J. Chem. Inf. Model.* **2013**. https://doi.org/10.1017/CBO9781107415324.004.

(14)   Perkin-Elmer. Thermogravimetric Analysis (TGA) A Beginner ' S Guide. *PerkinElmer, Inc* **2010**, 1–19. https://doi.org/10.1007/978-0-387-93837-0.

(15)   Ngo, P. D. Energy Dispersive Spectroscopy. In *Failure Analysis of Integrated Circuits*; 1999. https://doi.org/10.1007/978-1-4615-4919-2_12.

(16)   Energy Dispersive X-Ray Spectroscopy (EDS) https://www.mee-inc.com/hamm/energy-dispersive-x-rayspectroscopyeds/.

(17)   Gabriel, B. L. *SEM: A User's Manual for Materials Science*; 1995.

(18)   Klein, L. C. *Sol-Gel Technology for Thin Fims, Fibers, Preforms, Electronics and Speciality Shapes*; 1998.

(19)   Cormier, D.; Williams, S. A. Aerosol Jet Printing. 2018.

(20)   Cormier, D. InkJet: On-Demand Digital Material Deposition. 2017.

(21)   Petrucci, R. H.; Harwood, W. S.; Herring, F. . *General Chemistry: Principles and Modern Applications*; 2002. https://doi.org/10.1007/s13398-014-0173-7.2.

(22)   Schroder, K. A. Mechanisms of Photonic Curing™: Processing High Temperature Films on Low Temperature Substrates. In *Nanotech Conference Technical Proceedings*; 2011.

(23)   Liu, G.; Zhang, S.; Jiang, W.; Cao, W. Losses in Ferroelectric Materials. *Materials Science and Engineering R: Reports*. 2015. https://doi.org/10.1016/j.mser.2015.01.002.

(24)   Chen, Caifeng., Hong, Daiwei., Wang, Andong., Ni, C. Fabrication of Flexible Piezoelectric PZT/Fabric Composite. *Sci. World J.* **2013**, *2013*, 1–4.

(25)   Park, K. Il; Son, J. H.; Hwang, G. T.; Jeong, C. K.; Ryu, J.; Koo, M.; Choi, I.; Lee, S. H.; Byun, M.; Wang, Z. L.; et al. Highly-Efficient, Flexible Piezoelectric PZT Thin Film Nanogenerator on Plastic Substrates. *Adv. Mater.* **2014**. https://doi.org/10.1002/adma.201305659.

(26)   Chakrabarti, N.; Maiti, H. S. Chemical Synthesis of PZT Powder by Auto-Combustion of Citrate - Nitrate Gel. *Mater. Lett.* **1997**. https://doi.org/10.1016/S0167-577X(96)00191-7.

(27)   Bel Hadj Tahar, R.; Bel Hadj Tahar, N.; Ben Salah, A. Preparation and Characterization of PZT Solid Solutions via Sol-Gel Process. *J. Cryst. Growth* **2007**. https://doi.org/10.1016/j.jcrysgro.2007.04.046.

(28)   Shakeri, A.; Abdizadeh, H.; Golobostanfard, M. R. Synthesis and Characterization of Thick PZT Films via Sol-Gel Dip Coating Method. *Appl. Surf. Sci.* **2014**. https://doi.org/10.1016/j.apsusc.2014.07.087.

(29)   Tsaur, J.; Wang, Z. J.; Zhang, L.; Ichiki, M.; Wan, J. W.; Maeda, R. Preparation and Application of Lead Zirconate Titanate (PZT) Films Deposited by Hybrid Process: Sol-Gel Method and Laser Ablation. *Japanese J. Appl. Physics, Part 1 Regul. Pap. Short Notes Rev. Pap.* **2002**.

https://doi.org/10.1143/JJAP.41.6664.

(30) Ouyang, J.; Cormier, D.; Williams, S. A.; Borkholder, D. A. Photonic Sintering of Aerosol Jet Printed Lead Zirconate Titanate (PZT) Thick Films. *J. Am. Ceram. Soc.* **2016**. https://doi.org/10.1111/jace.14272.

(31) Shoghi, A.; Shakeri, A.; Abdizadeh, H.; Golobostanfard, M. R. Synthesis of Crack-Free PZT Thin Films by Sol-Gel Processing on Glass Substrate. *Procedia Mater. Sci.* **2015**. https://doi.org/10.1016/j.mspro.2015.11.136.

(32) Yao, Kui., Shuhui Yu., Eng-Hock Tay, F. Residual Stress Snalysis in Ferroelectric Pb (Zr.52 Ti .48)O3 Thin Films Fabricated by a Sol-Gel Process. *Appl. Physcis* **2003**, *82* (4540).

(33) Yu, S.; Yao, K.; Shannigrahi, S.; Hock, F. T. E. Effects of Poly(ethylene Glycol) Additive Molecular Weight on the Microstructure and Properties of Sol-Gel-Derived Lead Zirconate Titanate Thin Films. *J. Mater. Res.* **2003**, *18* (3), 737–741. https://doi.org/10.1557/JMR.2003.0100.

(34) Bahcer, A. Infrared Spectroscopy.

(35) Williams, S. A. Aerosol Jet Deposition and Fabrication of PZT Using a Sol-Gel Route (Personal Communications). 2017.

(36) Zak, A. K.; Majid, W. H. A.; Darroudia, M. Synthesis and Characterization of Sol-Gel Derived Singlephase PZT Nanoparticles in Aqueous Polyol Solution. *J. Optoelectron. Adv. Mater.* **2010**, *12* (8), 1714–1719.

(37) Solutions, I. D. Printing Parameters. 2018.

(38) Bainbridge, I. F.; Taylor, J. A. The Surface Tension of Pure Aluminum and Aluminum Alloys. *Metall. Mater. Trans. A Phys. Metall. Mater. Sci.* **2013**, *44* (8), 3901–3909. https://doi.org/10.1007/s11661-013-1696-9.

(39) Wang, D.; Guo, H.; Morandi, C. S.; Randall, C. A.; Trolier-McKinstry, S. Cold Sintering and Electrical Characterization of Lead Zirconate Titanate Piezoelectric Ceramics. *APL Mater.* **2018**. https://doi.org/10.1063/1.5004420.

(40) Additive Manufacturing Brochure.

(41) Saurez-Gomez, A., Saniger-Blesa, J.M., Caleron-Pinar, F. "Universal" Structures of PZT (1-x)/X Submicrometric Structures Using Highly Stable Colloidal Dispersions: A Bottom-Up Approach. *Adv. Ferroelectr.* **2012**.

(42) Datta, S. Piezoelectric Materials: Crystal Orientation & Poling Direction.

(43) Ouyang, J. Enhanced Piezoelectric Performance of Printed PZT Films on Low Temperature Substrates, Rochester Institute of Technology, 2014.